

Hyperfine Structure of Quantum Entanglement

Liang-Hong Mo,¹ Yao Zhou,¹ Jia-Rui Sun,^{2,*} and Peng Ye^{1,†}

¹Guangdong Provincial Key Laboratory of Magnetolectric Physics and Devices,
State Key Laboratory of Optoelectronic Materials and Technologies,
and School of Physics, Sun Yat-sen University, Guangzhou, 510275, China

²School of Physics and Astronomy, Sun Yat-sen University, Guangzhou, 510275, China
(Dated: June 12, 2024)

Quantum entanglement, crucial for understanding quantum many-body systems and quantum gravity, is commonly assessed through various measures such as von Neumann entropy, mutual information, and entanglement contour, each with its inherent limitations. In this work, we introduce the *hyperfine structure of entanglement*, which dissects entanglement contours known as the fine structure into particle-number cumulants. This measure exhibits a set of universal properties with its significance in quantum information science. We apply it across diverse contexts: in Fermi gases, establishing connections to mutual information and interacting conformal field theory; in AdS₃/CFT₂ holographic duality, unveiling finer subregion-subregion duality and extending bulk reconstruction; and in Chern insulators, distinguishing between different quantum phases. Our findings suggest experimental accessibility, offering fresh insights into quantum entanglement across physical systems.

Introduction.— Quantum entanglement, pivotal in quantum information, elucidates quantum many-body systems and gravity [1–8]. It propels quantum computation [9], unveils unconventional phases [10–12], and reveals gravity phenomena [13–15]. Various measures quantify entanglement, including von Neumann entropy, Rényi entropy, mutual information, and negativity [1], yet each has limitations. For instance, negativity may be zero even in an entangled state [16]. While mutual information detects mixed-state entanglement, it struggles to differentiate quantum from classical correlations, unlike entanglement entropy. Moreover, these measures fail to fully unveil the properties of $\hat{\rho}_A$, i.e., the entanglement spectrum and entanglement wave function (Schmidt vectors) [11, 17, 18]. It is always important to find more ways of measure to quantify entanglement.

Chen and Vidal first put forward an entanglement quantity called “entanglement contour” [19] that can be regarded as the *fine structure of entanglement* distribution in real space. More precisely, the entanglement entropy $S(A)$ between a subregion A and its complement \bar{A} is decomposed as the sum of entanglement contour $s(i)$ over all sites, expressed as $S(A) = \sum_{i \in A} s(i)$. Since then, the contour function $s(i)$ has been explored in various contexts: fractal lattice [20], Gaussian states [19], conformal field theory (CFT) [21, 22], geometric construction in the AdS/CFT correspondence, and partial entanglement entropy derived by the additive linear combination of subset entanglement entropy [23]. The extension to the n -th order Rényi entropy $S_n(A)$, defined as $S_n(A) = \frac{1}{1-n} \ln \text{tr} \hat{\rho}_A^n$, has also been explored by introducing the n -th order Rényi contour $s_n(i)$ [19, 21, 24, 25], as below:

$$\begin{array}{ccccc} S(A) & \implies & s(i) & \implies & h_{1;k}(i) \\ \uparrow n=1 & & \uparrow n=1 & & \uparrow n=1 \\ S_n(A)(\tilde{S}_n(A)) & \implies & s_n(i)(\tilde{s}_n(i)) & \implies & h_{n;k}(i)(\tilde{h}_{n;k}(i)) \end{array}$$

In this work, we significantly expand the zoo of entanglement quantities and uncover a deeper understanding of

quantum entanglement by introducing the *hyperfine structure of entanglement*. Specifically, we precisely decompose the fine structure of entanglement $s_n(i)$, into contributions from particle-number cumulants, i.e., $s_n(i) = \sum_{k=1}^{\infty} h_{n;k}(i)$ defined in Eq. (1). We rigorously prove that the hyperfine structure, represented by $h_{n;k}(i)$, is an exotic entanglement quantity with several universal properties, including additivity, normalization, exchange symmetry, and local unitary invariance, making the hyperfine structure physical and meaningful just like other quantum informative measures. We then apply this quantity to the following three distinct physical contexts, demonstrating plentiful findings.

First, in a Fermi gas, we find that $s_n(i) \approx h_{n;2}(i)$, with all $h_{n;k}$ for $k > 2$ being suppressed. Using this simplified relation, we establish the connection between $h_{n;2}$ and mutual information, showing that $h_{n;2}$ negatively contribute to the mutual information. We also generalize these results into generally interacting (1+1)D CFT. *Second*, from a holographic perspective, the hyperfine structure of entanglement unveils a finer subregion-subregion duality in the bulk reconstruction. Specifically, we demonstrate that the hyperfine structure of holographic *refined* Rényi entropy is dual to the density-density correlator in the boundary subregion. Surprisingly, for a given boundary subregion, the bulk extremal surfaces associated with refined Rényi entropy can extend beyond the entanglement wedge determined by entanglement entropy. It indicates that the holographic dual of refined Rényi entropy and its hyperfine structure can be utilized to construct bulk local operators outside the entanglement wedge. *Third*, by investigating a prototypical (2+1)D lattice model, we numerically observe significant distinctions in the hyperfine structure across parameter regions, such as trivial mass gap, topological gap (supporting edge states and nonzero bulk Chern number), Dirac critical point, and Fermi surface. This hyperfine structure, based on local measurement, is experimentally accessible, such as through a quantum point contact. We conclude by discussing several future directions based on these findings.

Definition and properties.— Focusing on free fermions with conserved charge, to introduce the hyperfine structure of entanglement, denoted as $h_{n;k}(j)$, we precisely decompose the

* sunjiarui@mail.sysu.edu.cn
† yepeng5@mail.sysu.edu.cn

n -th order Rényi contour $s_n(j)$ at site j in subsystem A according to the contribution from all particle-number cumulants (details in the supplementary material (SM) [26] section I):

$$s_n(j) \equiv \sum_{k=1}^{\infty} h_{n;k}(j) = \sum_{k=1}^{\infty} \left(\beta_k(n) C_k(j) \right), \quad (1)$$

where $\beta_k(n)$ is non-zero only for even k . $\beta_k(n) = \frac{2}{n-1} \frac{1}{k!} \left(\frac{2\pi i}{n} \right)^k \zeta \left(-k, \frac{n+1}{2} \right)$, with $\zeta \left(-k, \frac{n+1}{2} \right)$ as the Hurwitz zeta function [27]. For instance, $\beta_2(2) = \frac{\pi^2}{4}$, $\beta_4(2) = -\frac{\pi^4}{192}$, and so forth. Here, the density of cumulant $C_k(j)$ on site j is defined as

$$C_k(j) \equiv (-i\partial_\lambda)^{k-1} \frac{\langle \exp(i\lambda \hat{N}_A) \hat{n}_j \rangle}{\langle \exp(i\lambda \hat{N}_A) \rangle} \Big|_{\lambda=0}, \quad (2)$$

where \hat{n}_j represents the particle-number operator at site j , \hat{N}_A is the total particle-number operator for the subsystem A , and λ is a real number. We observe that $C_k(j)$ corresponds to the $2k$ -point correlation function. The first non-zero term $C_2(j)$ simplifies to $C_2(j) = \sum_i \langle \hat{n}_i \hat{n}_j \rangle - \langle \hat{n}_i \rangle \langle \hat{n}_j \rangle$. The complete set of $C_k(j)$ with even k can be utilized to obtain the complete set of $s_n(j)$ based on Eq. (1). Interestingly, this process is reversible when a cutoff is applied, as we can use information about $s_n(j)$ to reconstruct the set of $C_k(j)$.

Moreover, the hyperfine structure $h_{n;k}(j)$ defined in Eq. (1) exhibits several universal properties as a quantum information quantity: **(i)**. Additivity. For $i, j \in A$, $h_{n;k}(i) + h_{n;k}(j) = h_{n;k}(i \cup j)$. **(ii)**. Normalization. The sum of $h_{n;k}(j)$ over all sites in A equals the *particle-number cumulant* C_k , specifically, $C_k = \sum_j h_{n;k}(j) / \beta_k(n)$. Here, C_k is defined as $C_k \equiv (-i\partial_\lambda)^k \ln \chi(\lambda, \hat{N}_A) \Big|_{\lambda=0}$, with the generating function $\chi(\lambda, \hat{N}_A) \equiv \langle \exp(i\lambda \hat{N}_A) \rangle$. **(iii)**. Exchange symmetry. If \hat{T} represents a symmetry of the reduced density matrix $\hat{\rho}_A$ and satisfies $\hat{T} \hat{\rho}_A \hat{T}^\dagger = \hat{\rho}_A$, and \hat{T} exchanges site i with site j , then $h_{n;k}(i) = h_{n;k}(j)$. **(iv)**. Local unitary Invariance. If the quantum state transforms from $|\psi\rangle$ to $|\psi'\rangle$ using a unitary transformation \hat{U}^X acting on a subset $X \subset A$, then $h_{n;k}(j \in X)$ remains the same for both states $|\psi\rangle$ and $|\psi'\rangle$. Notably, both $h_{n;k}(j)$ and $C_k(j)$ can be either negative or positive, but $s_n(j)$ must be positive.

Fermi gas.— We first apply the hyperfine structure to the $(d+1)$ D Fermi gas in continuum spacetime. We find that the sum of all $h_{n;k}$ with $k > 2$ vanishes, simplifying the exact expression in Eq. (1) to (see SM [26] section II):

$$\frac{s_n(x)}{h_{n;2}(x)} = 1 + o(1), \quad (3)$$

where

$$h_{n;2}(x) = \beta_k(n) \int_{y \in A} [\langle \hat{n}(x) \hat{n}(y) \rangle - \langle \hat{n}(x) \rangle \langle \hat{n}(y) \rangle] dy. \quad (4)$$

Here, $\hat{n}(x)$ denotes the particle-number operator at position x , and $o(1)$ denotes a term negligible compared to 1. This simplified expression is closely related to the mutual information

$I_2(A_1, A_2) \equiv S(A_1) + S(A_2) - S(A_1 \cup A_2)$ between regions A_1 and A_2 (see Fig. 1(a)) through

$$I_2(A_1, A_2) = 2 \left(S(A_1) - \int_{x \in A_1} h_{1;2}(x) dx \right), \quad (5)$$

where $h_{1;2}(x)$ is the hyperfine structure of region $A_1 \cup A_2 = A$. It is obvious that the integral of hyperfine structure negatively contributes to the mutual information between A_1 and A_2 . More intriguingly, with the entropy and hyperfine structure of subregion A_1 , we can derive the mutual information $I_2(A_1, A_2)$ without needing to consider any additional properties of A_2 .

To proceed further, we explicitly derive the hyperfine structure in a $(1+1)$ D CFT as an example, which is useful in the next section. We consider the action of free Dirac Fermions, given by $S = \frac{1}{2} \int d^2x \bar{\psi} \gamma_\mu \partial^\mu \psi$, where $\psi = (\psi_R, \psi_L)^T$. The corresponding correlation functions are $\langle \psi_R^\dagger(z) \psi_R(\omega) \rangle = -\frac{1}{2\pi} \frac{1}{z-\omega}$, $\langle \psi_L^\dagger(\bar{z}) \psi_L(\bar{\omega}) \rangle = -\frac{1}{2\pi} \frac{1}{\bar{z}-\bar{\omega}}$. Considering A as an interval with $x \in (-R + \epsilon, R - \epsilon)$ on an infinite line (where R is A 's radius and ϵ is the UV cutoff), we have the dominant hyperfine structure as

$$h_{n;2}(x) = \frac{(1+n^{-1})}{12} \left(\frac{1}{R-x} + \frac{1}{R+x} \right). \quad (6)$$

By integrating $s_n(x)$ over A , we can obtain the Rényi entropy as $S_n = \int_{-R+\epsilon}^{R-\epsilon} dx s_n(x) \approx [(1+n^{-1})/6] \ln \frac{2R}{\epsilon}$. Comparing the known equality $S_n = [(1+n^{-1})c/6] \ln \frac{2R}{\epsilon}$, we end up with the value of the central charge $c = 1$, which agrees with the known fact of free Dirac fermions models. Interestingly, we observe that the dominant hyperfine structure $h_{n;2}$ is independent of the UV cutoff, unlike Rényi entropy S_n .

Holographic duality.— From the AdS/CFT correspondence, the entanglement entropy of a boundary subregion A can be determined by the extremal surface (homologous to the boundary of A) in bulk AdS spacetime, which is called the Ryu-Takayanagi (RT) surface \mathcal{E}_A [13, 28] in Fig. 1(c). It is natural to ask what the holographic duality of the hyperfine structure is.

In the following we will answer this question by considering the refined Rényi entropy $\tilde{S}_n \equiv n^2 \partial_n \left(\frac{n-1}{n} S_n \right)$, which has been shown to be dual to the cosmic brane in the bulk AdS spacetime [29]. The relation between particle-number fluctuation and Rényi contour in Eq. (3) can be rewritten for the n -th refined Rényi contour as

$$\tilde{s}_n(x) \approx \tilde{h}_{n;2}(x) = \frac{\pi^2}{3n} \int_{y \in A} dy [\langle \hat{n}(x) \hat{n}(y) \rangle - \langle \hat{n}(x) \rangle \langle \hat{n}(y) \rangle]. \quad (7)$$

It is crucial to recognize that although Eq. (7) is initially derived from the non-interacting Fermi gases model, it is still valid for generally interacting CFTs up to a specific constant coefficient, as proved in SM [26] section II B. Thus, Eq. (7) remains applicable in the large central charge limit, which has the dual bulk classical gravity description [30].

To elucidate the holographic dual within the AdS₃ spacetime, we will employ the Rindler transformation [15]. The

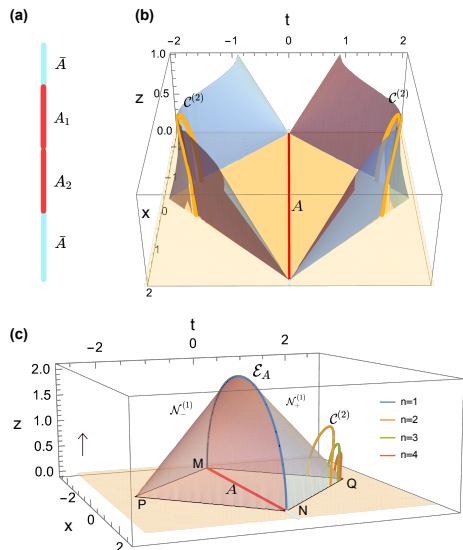


FIG. 1. (a) A tripartition of the system to calculate the mutual information $I_2(A_1, A_2)$, where A_1 and A_2 can be disjoint. In (c) ((b)), the two transparent surfaces are the null hypersurfaces $\mathcal{N}_\pm^{(1)}$ ($\mathcal{N}_\pm^{(2)}$), intersecting at the RT surface \mathcal{E}_A (the extremal surface $\mathcal{C}^{(2)}$). Discontinuities occur on the null hypersurfaces $\mathcal{N}_\pm^{(n \neq 1)}$ due to conical defect and the backreaction from $\mathcal{C}^{(n)}$. These singularities vanish when $n = 1$. For $n \geq 2$, the intersections of $\mathcal{N}_\pm^{(n)}$ form $\mathcal{C}^{(n)}$, depicted as yellow, green, and orange curves for $n = 2, 3, 4$ respectively. Clusters of $\mathcal{C}^{(n)}$ appear on both sides of \mathcal{E}_A , though for clarity, only the clusters on the right are shown in (c). We set $R = 2$.

basic idea of Rindler transformation is to convert the entanglement entropy of a region into the thermal entropy of another region which can be mapped to the horizon entropy of a hyperbolic black hole. It turns out that the horizon corresponds to the null hypersurfaces $\mathcal{N}_\pm^{(1)}$ in the original AdS spacetime in Fig. 1(c). The intersection of these null hypersurfaces is the extremal surface \mathcal{E}_A . It can be shown that the refined Rényi entropy of $\hat{\rho}_A$ is equivalent to the entanglement entropy of the n -replica reduced density matrix $\tilde{\rho}_A \equiv \frac{(\hat{\rho}_A)^n}{\text{Tr}(\hat{\rho}_A)^n}$ (see SM [26] section III). Therefore, the intersection of the n -dependent null hypersurfaces $\mathcal{N}_\pm^{(n)}$ is the holographic dual of \tilde{S}_n in Fig. 1(b) and (c). Notably, within the entanglement wedge enclosed by the boundary $PMQN$ and \mathcal{E}_A , the bulk operators can be reconstructed from the boundary CFT, which is the celebrated subregion-subregion duality in holographic duality [31].

Based on the holographic duality of extremal surfaces, it is natural to use planes connecting the boundary sites to slice $\mathcal{C}^{(n)}$ according to the distribution in Eq. (7), thereby deriving the holographic dual of the hyperfine structure. Each segment derived from the extremal surface represents the holographic dual of the hyperfine structure. Thus, the holographic description of Rényi entropy is refined into the duality between the boundary density-density correlator and the segment of bulk extremal surface. This finer correspondence indicates that the bulk local operator can be determined by finer subregion on the boundary.

More excitingly, $\mathcal{C}^{(n)}$ lies outside the entanglement wedge, thus the hyperfine structure provides a finer description for the subregion-subregion duality beyond the entanglement wedge. It is noteworthy that $\mathcal{C}^{(n)}$ with $n > 1$ differ markedly from the $n = 1$ RT surface \mathcal{E}_A . Firstly, $\mathcal{C}^{(n)}$ are inclined in the time direction and exhibit a conical defect, manifesting as discontinuous regions in $\mathcal{N}_\pm^{(n)}$. Secondly, $\mathcal{C}^{(n)}$ cannot be connected to \mathcal{E}_A through time evolution, since time unitary evolution does not modify the entanglement spectrum of a density matrix. Based on these observation, we can further define the Rényi entanglement wedge enclosed by $\mathcal{C}^{(n)}$. Intriguingly, this generalization extends the bulk reconstruction based on the entanglement wedge [32, 33], which allows the reconstruction of bulk local operators outside the entanglement wedge.

Chern insulators.— Next, we investigate the behavior of $s_n(j)$ and $h_{n;k}(j)$ in the $(2+1)$ D Chern insulator [34–36]: $\hat{\mathcal{H}} = \sum_{\mathbf{k}} \hat{c}_{\mathbf{k}}^\dagger H(\mathbf{k}) \hat{c}_{\mathbf{k}}$, where $H(\mathbf{k}) = (m + \cos k_x + \cos k_y) \sigma_z + \lambda (\sin k_x \sigma_x + \sin k_y \sigma_y) - \mu \mathbf{I}$, σ_i represent the Pauli matrices and \mathbf{I} is the 2×2 identity matrix. This Hamiltonian comprises a Zeeman splitting term induced by the mass parameter m and a spin-orbit coupling term with amplitude λ . The energy gap closes at $m = \pm 2$, forming a Dirac point respectively at $\mathbf{k} = (0, 0)$ and $\mathbf{k} = (\pi, \pi)$. For $m = 0$, the energy gaps close, creating two Dirac points with vanishing density-of-states: one at $\mathbf{k} = (0, \pi)$ and the other at $\mathbf{k} = (\pi, 0)$. In the following, we consider four distinct scenarios: (i) trivial mass gap; (ii) topological mass gap (supporting nonzero Chern number and robust edge states); (iii) critical Dirac point; (iv) Fermi surface.

Fig. 2 displays the distributions of $s_n(j)$, $h_{n;2}(j)$, $h_{n;4}(j)$, and $h_{n;6}(j)$ for various types of parameters. The four rows correspond to cases of trivial mass gap, topological mass gap, critical Dirac point, and Fermi surface. The four columns represent different terms of the hyperfine structure. Notably, the behavior of $h_{n;k>6}$ resembles that of $h_{n;4}(j)$ and $h_{n;6}(j)$, thus we focus on the first three non-zero terms $h_{n;2,4,6}(j)$.

Examining the first two columns within each row, we observe that the distribution and magnitude of $s_n(j)$ and $h_{n;2}(j)$ are very similar, indicating that $h_{n;2}$ is dominant in the series $h_{n;k}$. This aligns with previous findings [37] showing a numerical resemblance between the entanglement contour and the density of \mathcal{C}_2 . In addition to this observation, we find more interesting features as follows.

Comparing the distribution of $h_{n;2}(j)$ across the three system types, we note that in cases of mass gap (either trivial or topological) and critical points, $h_{n;2}(j)$ decays more rapidly from the boundary of A to the center of A compared to the Fermi surface case. Upon further investigation, we find that in cases of mass gap (either trivial or topological), $h_{n;2}(j)$ decays exponentially from the boundary to the center. However, in the cases of critical points and Fermi surfaces, $h_{n;2}(j)$ decays according to a power law but with different power law exponents (See SM [26] section IV).

As Eq. (1) enables the analysis of contributions from all values of k , we examine the hyperfine structure $h_{n;k}(j)$ for larger k ($k > 2$), as depicted in the third and fourth columns, where negative values of $h_{n;k}(j)$ are observed. In the trivial mass gap scenario, for any given n and k , the values of $h_{n;k}(j)$

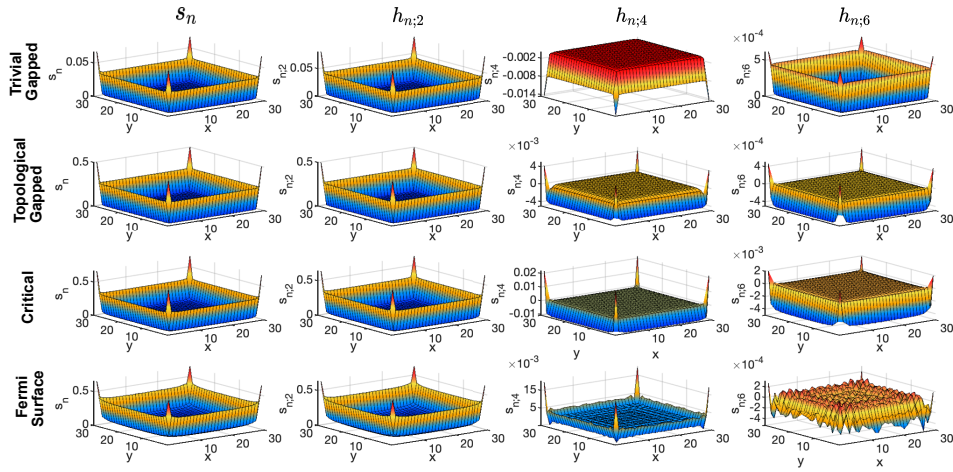


FIG. 2. Distribution of $s_n(j)$ and $h_{n;k}(j)$ for different types of energy spectra in a 60×60 lattice model with periodic boundary conditions in both x and y coordinates. Region A contains 30×30 sites. The first row shows the case of a trivial mass gap with $m = 3$ and chemical potential $\mu = 0$, the second row shows the case of a topological gap with $m = 1, \mu = 0$, the third row shows the case of critical point with $m = 0, \mu = 0$, and the last row shows the case of a Fermi surface with $m = 0$ and $\mu = 2/3$. We consider $n = 2$ and $\lambda = 1$ in all cases. The four columns represent the distributions of $s_n(j)$, $h_{n;2}(j)$, $h_{n;4}(j)$, and $h_{n;6}(j)$, respectively.

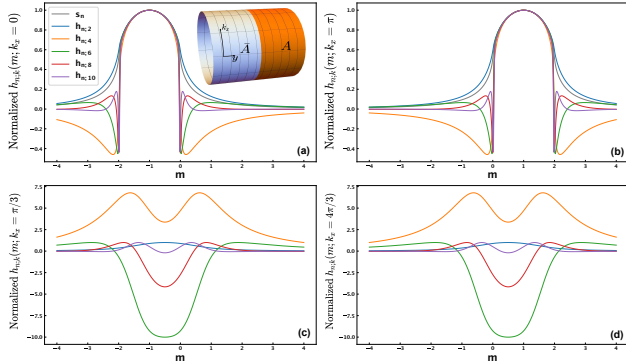


FIG. 3. Normalized $h_{n;k}(m; k_x)$ as a function of m : (a) $k_x = 0$, (b) $k_x = \pi$, (c) $k_x = \pi/3$, and (d) $k_x = 4\pi/3$. We set $n = 2$ and $\lambda = 1$ for generality.

for the whole A maintain consistent sign across all sites j , with corner and hinge sites sharing the same sign. However, in both cases of topological mass gap and critical Dirac point, the sign of $h_{n;k}(j)$ at corner sites may be different from the sign at hinge sites. In this way, we can distinguish the case of trivial mass gap from critical point and topological mass gap.

From the distribution of hyperfine structure in Fig. 2, the behaviour of topological phase is similar to the critical point. To further detect the topological edge modes, we vary the parameter m across different phases using the partition scheme shown in the upper-right of Fig. 3(a), where the y -axis is an open boundary and the x -axis is periodic. We compute $h_{n;k}$ from the edge of region A as a function of m , denoted by $h_{n;k}(m; k_x) = h_{n;k}(m; k_x, y \in \partial A)$, where k_x is the momentum quantum number along the x -axis and ∂A are the sites near the boundary cut between A and \bar{A} . To ensure a fair comparison and mitigate variations in magnitude, we normalize boundary $h_{n;k}$ by its maximum as

$h_{n;k}(m; k_x) / \max h_{n;k}(m; k_x)$. This normalization process is applied uniformly to all k_x .

We observe that most of the normalized $h_{n;k}(m; k_x)$ are randomly distributed, as shown in Fig. 3(c) and (d) for $k_x = \pi/3$ and $k_x = 4\pi/3$, except for those with $k_x = 0$ and $k_x = \pi$. For these special cases, as seen in Fig. 3(a) and (b), $h_{n;k}(m; k_x)$ with different k converge to a single curve and reach their maximum values for m values in the intervals of $(-2, 0)$ and $(0, 2)$. The emergence of this scaling law within the topological mass gap regions, namely $m \in (-2, 0) \cup (0, 2)$, indicates the existence of critical edge states and a fundamental $1/2$ mode in the entanglement spectrum. This $1/2$ mode represents the most entangled and correlated mode for $h_{n;k}$ across all values of k and corresponds to the edge states in lattice fermion models. It is essentially the Einstein–Podolsky–Rosen (EPR) pair that contributes the maximum entanglement. In summary, these distribution properties highlight the different features of a mass gap, a critical Dirac cone, and a Fermi surface, and they reveal a universal scaling behavior in the presence of topological edge states. These discussions can be generalized to a wider class of systems, including other Chern insulators and those with symmetry-protected topological order.

Outlook.— We suggest an experimental protocol based on quantum point contact, akin to prior work [17] (see SM [26] section V). The density-density correlators (Eq.(1)) can be measured using atomic quantum gases [38] and trapped ions [39], offering insights into entanglement spectra and system properties. The hyperfine structure relates the pre-measurement single-particle state to the post-measurement state, which is relevant to quantum state manipulation. Theoretical avenues include broader applications, discussions on correlated models, exploring the connection between the inclined extremal surface and the emergent tension within AdS₃/CFT₂ correspondence, and studying the effects of

measurement-based operations on the Rényi contour in quantum computations.

Acknowledgements.— This work was supported in part by NSFC Grant No. 12074438 and No. 11675272, the Guang-

dong Provincial Key Laboratory of Magnetoelectric Physics and Devices under Grant No. 2022B1212010008, and the (national) college students innovation and entrepreneurship training program, Sun Yat-sen University.

-
- [1] Ryszard Horodecki, Paweł Horodecki, Michał Horodecki, and Karol Horodecki, “Quantum entanglement,” *Reviews of Modern Physics* **81**, 865–942 (2009), arXiv:quant-ph/0702225 [quant-ph].
- [2] Luigi Amico, Rosario Fazio, Andreas Osterloh, and Vlatko Vedral, “Entanglement in many-body systems,” *Rev. Mod. Phys.* **80**, 517–576 (2008).
- [3] J. Eisert, M. Cramer, and M. B. Plenio, “Colloquium: Area laws for the entanglement entropy,” *Rev. Mod. Phys.* **82**, 277–306 (2010).
- [4] Nicolas Laflorencie, “Quantum entanglement in condensed matter systems,” *Physics Reports Quantum Entanglement in Condensed Matter Systems*, **646**, 1–59 (2016).
- [5] Mukund Rangamani, Tadashi Takayanagi, Mukund Rangamani, and Tadashi Takayanagi, *Holographic entanglement entropy* (Springer, 2017).
- [6] Ahmed Almheiri, Thomas Hartman, Juan Maldacena, Edgar Shaghoulian, and Amirhossein Tajdini, “The entropy of Hawking radiation,” *Rev. Mod. Phys.* **93**, 035002 (2021).
- [7] Thomas Faulkner, Thomas Hartman, Matthew Headrick, Mukund Rangamani, and Brian Swingle, “Snowmass white paper: Quantum information in quantum field theory and quantum gravity,” (2022), arXiv:2203.07117 [hep-th, physics:quant-ph].
- [8] Zhi-Kang Lin, Yao Zhou, Bin Jiang, Bing-Quan Wu, Li-Mei Chen, Xiao-Yu Liu, Li-Wei Wang, Peng Ye, and Jian-Hua Jiang, “Measuring entanglement entropy and its topological signature for phononic systems,” *Nature Communications* **15**, 1601 (2024), arXiv:2312.08632 [quant-ph].
- [9] John Preskill, “Quantum Computing in the NISQ era and beyond,” *Quantum* **2**, 79 (2018), arXiv:1801.00862 [quant-ph].
- [10] Michael Levin and Xiao-Gang Wen, “Detecting Topological Order in a Ground State Wave Function,” *Phys. Rev. Lett.* **96**, 110405 (2006), arXiv:cond-mat/0510613 [cond-mat.str-el].
- [11] Hui Li and F. D. M. Haldane, “Entanglement Spectrum as a Generalization of Entanglement Entropy: Identification of Topological Order in Non-Abelian Fractional Quantum Hall Effect States,” *Phys. Rev. Lett.* **101**, 010504 (2008), arXiv:0805.0332 [cond-mat.mes-hall].
- [12] Xiao-Liang Qi, Hoshio Katsura, and Andreas W. W. Ludwig, “General Relationship between the Entanglement Spectrum and the Edge State Spectrum of Topological Quantum States,” *Phys. Rev. Lett.* **108**, 196402 (2012), arXiv:1103.5437 [cond-mat.mes-hall].
- [13] Shinsei Ryu and Tadashi Takayanagi, “Holographic Derivation of Entanglement Entropy from the anti de Sitter Space/Conformal Field Theory Correspondence,” *Phys. Rev. Lett.* **96**, 181602 (2006), arXiv:hep-th/0603001 [hep-th].
- [14] Aitor Lewkowycz and Juan Maldacena, “Generalized gravitational entropy,” *Journal of High Energy Physics* **2013**, 90 (2013), arXiv:1304.4926 [hep-th].
- [15] Horacio Casini, Marina Huerta, and Robert C. Myers, “Towards a derivation of holographic entanglement entropy,” *Journal of High Energy Physics* **2011**, 36 (2011), arXiv:1102.0440 [hep-th].
- [16] Michał Horodecki, Paweł Horodecki, and Ryszard Horodecki, “Separability of mixed states: necessary and sufficient conditions,” *Physics Letters A* **223**, 1–8 (1996), arXiv:quant-ph/9605038 [quant-ph].
- [17] Israel Klich and Leonid Levitov, “Quantum Noise as an Entanglement Meter,” *Phys. Rev. Lett.* **102**, 100502 (2009), arXiv:0804.1377 [quant-ph].
- [18] H. Francis Song, Stephan Rachel, and Karyn Le Hur, “General relation between entanglement and fluctuations in one dimension,” *Phys. Rev. B* **82**, 012405 (2010), arXiv:1002.0825 [cond-mat.stat-mech].
- [19] Yangang Chen and Guifre Vidal, “Entanglement contour,” *Journal of Statistical Mechanics: Theory and Experiment* **2014**, 10011 (2014), arXiv:1406.1471 [cond-mat.str-el].
- [20] Yao Zhou and Peng Ye, “Quantum Entanglement on Fractal Landscapes,” arXiv e-prints, arXiv:2311.01199 (2023), arXiv:2311.01199 [quant-ph].
- [21] John Cardy and Erik Tonni, “Entanglement Hamiltonians in two-dimensional conformal field theory,” *Journal of Statistical Mechanics: Theory and Experiment* **12**, 123103 (2016), arXiv:1608.01283 [cond-mat.stat-mech].
- [22] Erik Tonni, Javier Rodríguez-Laguna, and Germán Sierra, “Entanglement hamiltonian and entanglement contour in inhomogeneous 1D critical systems,” *Journal of Statistical Mechanics: Theory and Experiment* **4**, 043105 (2018), arXiv:1712.03557 [cond-mat.stat-mech].
- [23] Qiang Wen, “Fine structure in holographic entanglement and entanglement contour,” *Phys. Rev. D* **98**, 106004 (2018), arXiv:1803.05552 [hep-th].
- [24] Andrea Coser, Cristiano De Nobili, and Erik Tonni, “A contour for the entanglement entropies in harmonic lattices,” *Journal of Physics A Mathematical General* **50**, 314001 (2017), arXiv:1701.08427 [cond-mat.stat-mech].
- [25] Qiang Wen, “Formulas for partial entanglement entropy,” *Physical Review Research* **2**, 023170 (2020), arXiv:1910.10978 [hep-th].
- [26] See the supplementary materials for more information.
- [27] Frank WJ Olver, *NIST handbook of mathematical functions hardback and CD-ROM* (Cambridge university press, 2010).
- [28] Mukund Rangamani and Tadashi Takayanagi, *Holographic Entanglement Entropy*, Vol. 931 (2017).
- [29] Xi Dong, “The gravity dual of Rényi entropy,” *Nature Communications* **7**, 12472 (2016), arXiv:1601.06788 [hep-th].
- [30] Ofer Aharony, Steven S. Gubser, Juan Maldacena, Hiroshi Ooguri, and Yaron Oz, “Large N field theories, string theory and gravity,” *physrep* **323**, 183–386 (2000), arXiv:hep-th/9905111 [hep-th].
- [31] Matthew Headrick, Veronika E. Hubeny, Albion Lawrence, and Mukund Rangamani, “Causality & holographic entanglement entropy,” *Journal of High Energy Physics* **2014**, 162 (2014), arXiv:1408.6300 [hep-th].
- [32] Xi Dong, Daniel Harlow, and Aron C. Wall, “Reconstruction of Bulk Operators within the Entanglement Wedge in Gauge-Gravity Duality,” *Phys. Rev. Lett.* **117**, 021601 (2016), arXiv:1601.05416 [hep-th].
- [33] Yi-Yu Lin, Jia-Rui Sun, and Yuan Sun, “Surface growth

- scheme for bulk reconstruction and tensor network,” *Journal of High Energy Physics* **2020**, 83 (2020), arXiv:2010.01907 [hep-th].
- [34] Xiao-Liang Qi, Yong-Shi Wu, and Shou-Cheng Zhang, “Topological quantization of the spin Hall effect in two-dimensional paramagnetic semiconductors,” *Phys. Rev. B* **74**, 085308 (2006), arXiv:cond-mat/0505308 [cond-mat.mes-hall].
- [35] Xiao-Liang Qi and Shou-Cheng Zhang, “Topological insulators and superconductors,” *Reviews of Modern Physics* **83**, 1057–1110 (2011), arXiv:1008.2026 [cond-mat.mes-hall].
- [36] Ching-Kai Chiu, Jeffrey C. Y. Teo, Andreas P. Schnyder, and Shinsei Ryu, “Classification of topological quantum matter with symmetries,” *Reviews of Modern Physics* **88**, 035005 (2016), arXiv:1505.03535 [cond-mat.mes-hall].
- [37] Irénée Frérot and Tommaso Roscilde, “Area law and its violation: A microscopic inspection into the structure of entanglement and fluctuations,” *Phys. Rev. B* **92**, 115129 (2015), arXiv:1506.00545 [cond-mat.quant-gas].
- [38] Chen-Lung Hung, Xibo Zhang, Li-Chung Ha, Shih-Kuang Tung, Nathan Gemelke, and Cheng Chin, “Extracting density-density correlations from in situ images of atomic quantum gases,” *New Journal of Physics* **13**, 075019 (2011), arXiv:1105.0030 [cond-mat.quant-gas].
- [39] A. Elben, B. Vermersch, C. F. Roos, and P. Zoller, “Statistical correlations between locally randomized measurements: A toolbox for probing entanglement in many-body quantum states,” *Phys. Rev. A* **99**, 052323 (2019), arXiv:1812.02624 [quant-ph].
- [40] Ingo Peschel, “LETTER TO THE EDITOR: Calculation of reduced density matrices from correlation functions,” *Journal of Physics A Mathematical General* **36**, L205–L208 (2003), arXiv:cond-mat/0212631 [cond-mat].
- [41] H. Francis Song, Stephan Rachel, Christian Flindt, Israel Klich, Nicolas Laflorencie, and Karyn Le Hur, “Bipartite fluctuations as a probe of many-body entanglement,” *Phys. Rev. B* **85**, 035409 (2012), arXiv:1109.1001 [cond-mat.mes-hall].
- [42] Pasquale Calabrese, Mihail Mintchev, and Ettore Vicari, “Exact relations between particle fluctuations and entanglement in Fermi gases,” *EPL (Europhysics Letters)* **98**, 20003 (2012), arXiv:1111.4836 [cond-mat.stat-mech].
- [43] Viktor Eisler and Ingo Peschel, “Analytical results for the entanglement Hamiltonian of a free-fermion chain,” *Journal of Physics A Mathematical General* **50**, 284003 (2017), arXiv:1703.08126 [cond-mat.stat-mech].
- [44] Roger S. K. Mong and Vasudha Shivamoggi, “Edge states and the bulk-boundary correspondence in Dirac Hamiltonians,” *Phys. Rev. B* **83**, 125109 (2011), arXiv:1010.2778 [cond-mat.mes-hall].
- [45] Ari M. Turner, Yi Zhang, and Ashvin Vishwanath, “Band Topology of Insulators via the Entanglement Spectrum,” arXiv e-prints, arXiv:0909.3119 (2009), arXiv:0909.3119 [cond-mat.str-el].
- [46] Lukasz Fidkowski, “Entanglement Spectrum of Topological Insulators and Superconductors,” *Phys. Rev. Lett.* **104**, 130502 (2010), arXiv:0909.2654 [cond-mat.str-el].
- [47] C. Flindt, C. Fricke, F. Hohls, T. Novotný, K. Netočný, T. Brandes, and R. J. Haug, “Universal oscillations in counting statistics,” *Proceedings of the National Academy of Science* **106**, 10116–10119 (2009), arXiv:0901.0832 [cond-mat.mes-hall].
- [48] Michael A Nielsen and Isaac L Chuang, *Quantum computation and quantum information* (Cambridge university press, 2010).

Supplementary Materials

The Supplemental Material (SM) provides further discussions on the technical details and theoretical demonstrations that support the main text. The organization of the SM is as follows: Section I provides the derivation and properties of the hyperfine structure; Section II presents a detailed demonstration and discussion on the hyperfine structure in Fermi gas; Section III provides the derivation of the holographic duality of the hyperfine structure; Section IV discusses the distribution function of the hyperfine structure across different parameter regions of Chern insulator and demonstrates the scaling behavior due to the presence of topological edge states; Finally, Section V proposes a promising experimental setup for measuring the hyperfine structure and discusses the relation between pre-measurement states and post-measurement states through hyperfine structure.

I. DEFINITION AND PROPERTIES OF THE HYPERFINE STRUCTURE

In this section, we first provide a brief review of the entanglement in free-fermion models (see the supplementary material of Ref. [8] for detailed discussion), including some entanglement quantities like entanglement entropy, Rényi entropy and the *fine structure* of entanglement. We then introduce the *hyperfine structure* of entanglement to expand the zoo of entanglement quantities within the model.

A. Entanglement of free-fermion Models

The Hamiltonian of free-fermion system has a generic quadratic form written as

$$H = \sum_{i,j} \hat{c}_i^\dagger \mathcal{H}_{i,j} \hat{c}_j, \quad (8)$$

where \hat{c}_j^\dagger and \hat{c}_j are the creation and annihilation operator, respectively. Denote the vacuum state as $|0\rangle$, the density matrix of the ground state $|G\rangle$ can be written as

$$\hat{\rho} = |G\rangle\langle G|. \quad (9)$$

By tracing out the remaining region \bar{A} , we can obtain the reduced density matrix

$$\hat{\rho}_A = \frac{1}{Z} e^{-\hat{K}_A}, \quad \hat{K}_A = \sum_{i,j \in A} \hat{c}_i^\dagger H_{A i,j} \hat{c}_j, \quad (10)$$

where Z is a normalization constant. Based on Ref. [40], the matrix inside the entanglement Hamiltonian can be written as

$$H_A = \ln[M^{-1} - \mathbf{I}], \quad (11)$$

where \mathbf{I} is the identity matrix and M is the correlation function matrix defined as

$$M_{ij} \equiv \langle G | \hat{c}_i^\dagger \hat{c}_j | G \rangle. \quad (12)$$

The entanglement entropy of the subregion A is given by

$$S_1 = -\text{tr} \hat{\rho}_A \ln \hat{\rho}_A = -\sum_k [\xi_k \ln \xi_k + (1 - \xi_k) \ln(1 - \xi_k)], \quad (13)$$

and Rényi entropy is expressed as

$$S_n = \frac{1}{1-n} \text{tr} \hat{\rho}_A^n = \frac{1}{1-n} \sum_k \ln[\xi_k^n + (1 - \xi_k)^n], \quad (14)$$

where $\{\xi_k\}$ are the eigenvalues of correlation matrix M and the eigenvectors of M is $\{\psi_k\}$.

Besides entanglement entropy and Rényi entropy, Y. Chen and G. Vidal have introduced another measure of entanglement known as the *entanglement contour* [19], the summation of which equates to the entanglement entropy. The entanglement contour represents the *fine structure* of the entanglement, reflecting its real-space distribution, and can be extended to the Rényi contour.

Before discussing the derivation of the contour function, we first review the concept of the projection operator. In the single-particle representation of free-fermion systems, the projection operator is defined as $\hat{P}_l = |l\rangle\langle l|$, satisfying $(\hat{P}_l)^2 = \hat{P}_l$. We have

$$\hat{P}_l M \hat{P}_l = \sum_{i,j} \hat{P}_l \langle \psi | \hat{c}_i^\dagger \hat{c}_j | \psi \rangle \hat{P}_l = \langle \hat{\psi} | \hat{c}_l^\dagger \hat{c}_l | \psi \rangle = M_{ll}, \quad (15)$$

where i, j, l are real space indices. Since the correlation matrix $M_{ij} = \langle \hat{c}_i^\dagger \hat{c}_j \rangle$ can be diagonalized as Λ by a unitary matrix O , this above relation can also be written as

$$\begin{aligned} (\hat{P}_l M \hat{P}_l)_{ip} &= (\hat{P}_l O \Lambda O^\dagger \hat{P}_l)_{ip} \\ &= \sum_{jmn} \delta_{il} \delta_{ij} O_{jm} \Lambda_{mn} (O^\dagger)_{mn} \delta_{np} \delta_{pl} \\ &= \sum_m \delta_{il} O_{im} \Lambda_{mm} (O^\dagger)_{mp} \delta_{pl} \\ &= M_{ip} \delta_{il} \delta_{pl}. \end{aligned} \quad (16)$$

Besides, the following relation is also useful:

$$\begin{aligned} (\hat{P}_l M^2 \hat{P}_l)_{ip} &= (\hat{P}_l)_{ij} \langle \hat{c}_j^\dagger \hat{c}_m \rangle \langle \hat{c}_m^\dagger \hat{c}_n \rangle (\hat{P}_l)_{np} \\ &= \sum_{jmn} \delta_{il} \delta_{ij} M_{jm} M_{mn} \delta_{np} \delta_{pl} \\ &= \sum_m \delta_{il} M_{im} M_{mp} \delta_{pl} \\ &= (M^2)_{ip} \delta_{il} \delta_{pl}. \end{aligned} \quad (17)$$

We can also insert some arbitrary operators, such as D into the equation:

$$\begin{aligned} (\hat{P}_l M D M \hat{P}_l)_{ip} &= (\hat{P}_l)_{ij} \langle \hat{c}_j^\dagger \hat{c}_m \rangle D_{mq} \langle \hat{c}_q^\dagger \hat{c}_n \rangle (\hat{P}_l)_{np} \\ &= \sum_{jmnq} \delta_{il} \delta_{ij} M_{jm} D_{mq} M_{qn} \delta_{np} \delta_{pl} \\ &= \sum_{mq} \delta_{il} M_{im} D_{mq} M_{qp} \delta_{pl} \\ &= (M D M)_{ip} \delta_{il} \delta_{pl}. \end{aligned} \quad (18)$$

The entanglement entropy can be written as

$$\begin{aligned} S(A) &= -\text{tr}[M \ln M + (\mathbf{I} - M) \ln(\mathbf{I} - M)] \\ &= \sum_{ml} O_{ml} (f(\Lambda))_{ll} (O^\dagger)_{lm}, \quad f(x) = -x \ln x - (1-x) \ln(1-x). \end{aligned} \quad (19)$$

Applying the projection operator onto the above equation, we have

$$\begin{aligned} s(j) &= \sum_{mli} \delta_{im} O_{ml} (f(\Lambda))_{ll} (O^\dagger)_{lm} \delta_{mi} \delta_{ij} \\ &= \sum_l O_{jl} (f(\Lambda))_{ll} (O^\dagger)_{lj} \\ &= \sum_l (-\xi_l \ln \xi_l - (1-\xi_l) \ln(1-\xi_l)) |\psi_l(j)|^2, \end{aligned} \quad (20)$$

which is exactly the entanglement contour put forward in Ref. [19]. Therefore, the entanglement contour $s(j)$ and Rényi contour $s_n(j)$ between subregion A and \bar{A} can be written as

$$s(j) \equiv -\text{tr}\{\hat{P}_j [M \ln M + (\mathbf{I} - M) \ln(\mathbf{I} - M)]\}, \quad (21)$$

and

$$s_n(j) \equiv \frac{1}{1-n} \text{tr}\{\hat{P}_j \ln[M^n + (1-M)^n]\}. \quad (22)$$

One can easily checked that the summation of the contour function turns out to be the entropy

$$S_n(A) = \sum_{j \in A} s_n(j). \quad (23)$$

B. Derivation of the hyperfine structure (Eq. (1)-(2) of the main text)

In the following, we will introduce the hyperfine structure of entanglement by decomposing the fine structure $s_n(j)$. Denoted the particle-number operator in A as $\hat{N}_A \equiv \sum_{i \in A} \hat{c}_i^\dagger \hat{c}_i$ and its maximal expectation value, or equivalently, the sites of subregion A as \mathcal{N}_A . The Rényi contour $s_n(j)$ can be decomposed into the contribution from different particle-number cumulants as presented in Eq. (1) of the main text:

$$s_n(j) \equiv \sum_{k=1}^{\infty} h_{n;k}(j) = \sum_{k=1}^{\infty} \left(\beta_k(n) C_k(j) \right) \quad (24)$$

where

$$C_k(j) \equiv (-i\partial_\lambda)^{k-1} \frac{G(\lambda, j)}{\chi(\lambda, \mathcal{N}_A)} \Big|_{\lambda=0}. \quad (25)$$

The denominator in Eq. (25) is the cumulant generating function $\chi(\lambda, \mathcal{N}_A) \equiv \langle \exp(i\lambda \hat{N}_A) \rangle$ and we also introduce a function defined as follows:

$$G(\lambda, j) \equiv \langle \exp(i\lambda \hat{N}_A) \hat{n}_j \rangle. \quad (26)$$

The summation of $C_k(j)$ over subregion A is given by the particle-number cumulant $C_k \equiv \sum_{j \in A} C_k(j)$ and one can easily check that $C_k = (-i\partial_\lambda)^k \ln \chi(\lambda, \mathcal{N}_A) \Big|_{\lambda=0}$.

Proof. Using the projection operator, we can also obtain the following useful conclusion

$$\sum_m \hat{P}_j \langle \exp(i\lambda \hat{N}_A) \hat{c}_m^\dagger \hat{c}_m \rangle \hat{P}_j = \langle \exp(i\lambda \hat{N}_A) \hat{c}_j^\dagger \hat{c}_j \rangle, \quad (27)$$

which we will demonstrate later. According to the Ref.[41], Rényi entropy defined as Eq. (19) can be written as the summation of particle-number cumulants as follows

$$\begin{aligned} S_n &= \frac{1}{1-n} \sum_{k=1}^{\infty} \beta_k(n) C_k \\ &= \frac{1}{1-n} \sum_{k=1}^{\infty} \beta_k(n) (-i\partial_\lambda)^k \ln \chi(\lambda) \Big|_{\lambda=0} \\ &= \frac{1}{1-n} \sum_{k=1}^{\infty} \beta_k(n) (-i\partial_\lambda)^{k-1} \frac{\langle \exp(i\lambda \hat{N}_A) \hat{N}_A \rangle}{\langle \exp(i\lambda \hat{N}_A) \rangle} \Big|_{\lambda=0}. \end{aligned} \quad (28)$$

We can also define the cumulant dissemination of S_n as $S_n = \sum_k^{\infty} h_{n;k}$, $h_{n;k} \equiv \frac{1}{1-n} \beta_k(n) C_k$. By applying the projection operator on both sides of Eq. (28) and referring to the Eq. (27), we have

$$\begin{aligned} \hat{P}_j S_n \hat{P}_j &= \frac{1}{1-n} \sum_{k=1}^{\infty} \beta_k(n) \sum_m (-i\partial_\lambda)^{k-1} \hat{P}_j \frac{\langle \exp(i\lambda \hat{N}_A) \hat{c}_m^\dagger \hat{c}_m \rangle}{\langle \exp(i\lambda \hat{N}_A) \rangle} \hat{P}_j \Big|_{\lambda=0} \\ &= \frac{1}{1-n} \sum_{k=1}^{\infty} \beta_k(n) (-i\partial_\lambda)^{k-1} \frac{\langle \exp(i\lambda \hat{N}_A) \hat{n}_j \rangle}{\langle \exp(i\lambda \hat{N}_A) \rangle} \Big|_{\lambda=0} \end{aligned} \quad (29)$$

Therefore, we demonstrate that the Rényi contour defined in Eq. (22) can be written as

$$s_n(j) = \sum_k h_{n;k}(j), \quad (30)$$

where we define the hyperfine structure of entanglement as

$$h_{n;k}(j) = \frac{1}{1-n} \sum_{k=1}^{\infty} \beta_k(n) (-i\partial_\lambda)^{k-1} \frac{\langle \exp(i\lambda \hat{N}_A) \hat{n}_j \rangle}{\langle \exp(i\lambda \hat{N}_A) \rangle} \Big|_{\lambda=0}. \quad (31)$$

In the following, we will demonstrate the Eq. (27).

Proof. The proof primarily relies on the equation $\langle e^{i\lambda(\sum_{i=1}^{\mathcal{N}_A} c_i^\dagger c_i)} c_l^\dagger c_l \rangle = e^{i\lambda} \langle e^{i\lambda(\sum_{i=1, i \neq l}^{\mathcal{N}_A} c_i^\dagger c_i)} c_l^\dagger c_l \rangle$, which we will demonstrate first.

$$\begin{aligned} \sum_l \langle e^{i\lambda(\sum_{i=1}^{\mathcal{N}_A} c_i^\dagger c_i)} c_l^\dagger c_l \rangle &= \left\langle \left(\prod_{i=1}^{\mathcal{N}_A} [1 + (e^{i\lambda} - 1) c_i^\dagger c_i] \right) c_l^\dagger c_l \right\rangle \\ &= \left\langle \left(\prod_{i=1, i \neq l}^{\mathcal{N}_A} [1 + (e^{i\lambda} - 1) c_i^\dagger c_i] \right) [1 + (e^{i\lambda} - 1) c_l^\dagger c_l] c_l^\dagger c_l \right\rangle \\ &= \left\langle \left(\prod_{i=1, i \neq l}^{\mathcal{N}_A} [1 + (e^{i\lambda} - 1) c_i^\dagger c_i] \right) [c_l^\dagger c_l + (e^{i\lambda} - 1)(c_l^\dagger c_l - c_l^\dagger c_l c_l c_l)] \right\rangle \\ &= \left\langle \left(\prod_{i=1, i \neq l}^{\mathcal{N}_A} [1 + (e^{i\lambda} - 1) c_i^\dagger c_i] \right) [c_l^\dagger c_l + (e^{i\lambda} - 1) c_l^\dagger c_l] \right\rangle \\ &= e^{i\lambda} \left\langle \left(\prod_{i=1, i \neq l}^{\mathcal{N}_A} [1 + (e^{i\lambda} - 1) c_i^\dagger c_i] \right) c_l^\dagger c_l \right\rangle \\ &= e^{i\lambda} \langle e^{i\lambda(\sum_{i=1, i \neq l}^{\mathcal{N}_A} c_i^\dagger c_i)} c_l^\dagger c_l \rangle. \end{aligned} \quad (32)$$

(1). When the subregion A only contains one site j , that is $\hat{N}_A = \hat{n}_j$,

$$\begin{aligned} \sum_m \hat{P}_j \langle \exp(i\lambda \hat{N}_A) \hat{c}_m^\dagger \hat{c}_m \rangle \hat{P}_j &= \hat{P}_j \langle [1 + (e^{i\lambda} - 1) \hat{c}_j^\dagger \hat{c}_j] \hat{c}_j^\dagger \hat{c}_j \rangle \hat{P}_j \\ &= \hat{P}_j \langle e^{i\lambda \hat{c}_j^\dagger \hat{c}_j} \rangle \hat{P}_j \\ &= \langle \exp(i\lambda \hat{N}_A) \hat{c}_j^\dagger \hat{c}_j \rangle. \end{aligned} \quad (33)$$

(2). When the subregion A contains two sites i, j , the process is similar.

$$\begin{aligned}
& \sum_l \hat{P}_j \langle \exp(i\lambda \hat{N}_A) \hat{c}_l^\dagger \hat{c}_l \rangle \hat{P}_j \\
&= \sum_l \hat{P}_j \langle [1 + (e^{i\lambda} - 1) \hat{c}_i^\dagger \hat{c}_i] [1 + (e^{i\lambda} - 1) \hat{c}_j^\dagger \hat{c}_j] \hat{c}_l^\dagger \hat{c}_l \rangle \hat{P}_j \\
&= \sum_l \hat{P}_j \langle [1 + (e^{i\lambda} - 1) \hat{c}_l^\dagger \hat{c}_l] e^{i\lambda} \hat{c}_l^\dagger \hat{c}_l \rangle \hat{P}_j \\
&= \sum_l e^{i\lambda} \hat{P}_j \left[\langle \hat{c}_l^\dagger \hat{c}_l \rangle + (e^{i\lambda} - 1) \left(\langle \hat{c}_l^\dagger \hat{c}_l \rangle \langle \hat{c}_l^\dagger \hat{c}_l \rangle - \langle \hat{c}_l^\dagger \hat{c}_l \rangle \langle \hat{c}_l^\dagger \hat{c}_l \rangle \right) \right] \hat{P}_j \\
&= e^{i\lambda} \left[\langle \hat{c}_j^\dagger \hat{c}_j \rangle + (e^{i\lambda} - 1) \left(\langle \hat{c}_j^\dagger \hat{c}_j \rangle \langle \hat{c}_i^\dagger \hat{c}_i \rangle - \langle \hat{c}_j^\dagger \hat{c}_i \rangle \langle \hat{c}_i^\dagger \hat{c}_j \rangle \right) \right] \\
&= \langle [1 + (e^{i\lambda} - 1) \hat{c}_i^\dagger \hat{c}_i] e^{i\lambda} \hat{c}_j^\dagger \hat{c}_j \rangle \\
&= \langle [1 + (e^{i\lambda} - 1) \hat{c}_i^\dagger \hat{c}_i] [1 + (e^{i\lambda} - 1) \hat{c}_j^\dagger \hat{c}_j] \hat{c}_j^\dagger \hat{c}_j \rangle \\
&= \langle \exp(i\lambda \hat{N}_A) \hat{c}_j^\dagger \hat{c}_j \rangle, \tag{34}
\end{aligned}$$

where \bar{l} is the site inside A but excludes the site l .

(3). The results can be easily extended to cases with any \mathcal{N}_A by recognizing the central role played by the Wick theorem:

$$\begin{aligned}
& \sum_l \hat{P}_j \langle \exp(i\lambda \hat{N}_A) \hat{c}_l^\dagger \hat{c}_l \rangle \hat{P}_j \\
&= \sum_l \hat{P}_j \left\langle \left(\prod_{i=1, i \neq l}^{\mathcal{N}_A} [1 + (e^{i\lambda} - 1) \hat{c}_i^\dagger \hat{c}_i] \right) e^{i\lambda} \hat{c}_l^\dagger \hat{c}_l \right\rangle \hat{P}_j \\
&= \sum_l e^{i\lambda} \hat{P}_j \left[\langle \hat{c}_l^\dagger \hat{c}_l \rangle + (e^{i\lambda} - 1) \left(\sum_{m \neq l} \left(\langle \hat{c}_l^\dagger \hat{c}_l \rangle \langle \hat{c}_m^\dagger \hat{c}_m \rangle - \langle \hat{c}_l^\dagger \hat{c}_m \rangle \langle \hat{c}_m^\dagger \hat{c}_l \rangle \right) \langle \dots \rangle + \sum_{p \neq l, q \neq l} \langle \hat{c}_l^\dagger \hat{c}_p \rangle \langle \hat{c}_q^\dagger \hat{c}_l \rangle \langle \dots \rangle \right) \right] \hat{P}_j \\
&= e^{i\lambda} \left[\langle \hat{c}_j^\dagger \hat{c}_j \rangle + (e^{i\lambda} - 1) \left(\sum_{m \neq j} \left(\langle \hat{c}_j^\dagger \hat{c}_j \rangle \langle \hat{c}_m^\dagger \hat{c}_m \rangle - \langle \hat{c}_j^\dagger \hat{c}_m \rangle \langle \hat{c}_m^\dagger \hat{c}_j \rangle \right) \langle \dots \rangle + \sum_{p \neq l, q \neq l} \langle \hat{c}_j^\dagger \hat{c}_p \rangle \langle \hat{c}_q^\dagger \hat{c}_j \rangle \langle \dots \rangle \right) \right] \hat{P}_j \\
&= \left\langle \left(\prod_{i=1, i \neq j}^{\mathcal{N}_A} [1 + (e^{i\lambda} - 1) \hat{c}_i^\dagger \hat{c}_i] \right) e^{i\lambda} \hat{c}_j^\dagger \hat{c}_j \right\rangle, \\
&= \langle \exp(i\lambda \hat{N}_A) \hat{c}_j^\dagger \hat{c}_j \rangle, \tag{35}
\end{aligned}$$

where $\langle \dots \rangle$ represents the coefficient part obtained using the Wick's theorem, excluding the contribution from $\hat{c}_l^\dagger, \hat{c}_l$ in the third row and $\hat{c}_j^\dagger, \hat{c}_j$ in the fourth row. □

□

Therefore, we demonstrated that fine structure in Eq. (22) can be decomposed into the hyperfine structure.

C. Information reconstruction from the fine structure $s_n(j)$

From the above sections, we know that the complete set of $h_{n;k}(j)$ with even k can be utilized to obtain the complete set of $s_n(j)$. In the following, we will demonstrate that the fine structure $s_n(j)$ can be used to reconstruct the sets of $C_k(j)$ when a cutoff is applied. Furthermore, based on the fine structure, we can derive the Rényi entropy, which allows us to reconstruct the entanglement spectra.

1. Particle-number correlation

Using Rényi Contour as the building block, we can reconstruct the information of the particle-number correlation. To illustrate this, consider a free-fermion system with \hat{N}_A fermions in subsystem A. Now, let's introduce a *cumulant coefficient matrix* denoted as B

$$B = \begin{pmatrix} \beta_2(1) & \beta_4(1) & \dots & \beta_{2\mathcal{N}_A}(1) \\ \beta_2(2) & \beta_4(2) & \dots & \beta_{2\mathcal{N}_A}(2) \\ \vdots & & \ddots & \\ \beta_2(\mathcal{N}_A) & \beta_4(\mathcal{N}_A) & \dots & \beta_{2\mathcal{N}_A}(\mathcal{N}_A) \end{pmatrix},$$

where $\beta_k(n)$ is non-zero only when k is even and $\beta_k(n) = \frac{2}{n-1} \frac{1}{k!} \left(\frac{2\pi i}{n}\right)^k \zeta\left(-k, \frac{n+1}{2}\right)$, then Eq. (1) of the main text can be written as

$$[s_1(j), s_2(j), \dots, s_{\mathcal{N}_A}(j)]^T = B[C_2(j), C_4(j), \dots, C_{2\mathcal{N}_A}(j)]^T. \quad (36)$$

By solving this linear algebra Eq. (36) inversely, we can reconstruct the even-rank particle-number fluctuation cumulants C_k with the cut off $k_c = 2\mathcal{N}_A$. Since C_k are the coefficient of the Taylor expansion $\chi(\lambda, \mathcal{N}_A) = \sum_{k=0}^{\infty} C_k \frac{\lambda^k}{k!}$, centered around $\lambda = 0$, the dominant C_k terms correspond to smaller values of k , such as the former k_c terms.

2. Entanglement spectrum

Besides the set of particle-number cumulant, Rényi contour can also be utilized to reconstruct the Rényi entropy and entanglement spectrum. The summation of Rényi contour over all sites yields the Rényi entropy, from which the entanglement spectrum can be derived.

Let T_n be the trace of the n -th power of the reduced density matrix [41]:

$$T_n = \text{tr}(\hat{\rho}_A^n) = e^{(1-n)S_n}. \quad (37)$$

Let us define $T_1 = 1$ for a normalized density matrix and introduce a $D \times D$ matrix as follows:

$$U = \begin{pmatrix} 1 & 1 & 0 & \dots & \\ T_2 & 1 & 2 & 0 & \dots \\ \vdots & \ddots & \ddots & \ddots & 0 \\ T_{D-1} & T_{D-2} & \dots & T_2 & D-1 \\ T_D & T_{D-1} & \dots & T_2 & 1 \end{pmatrix}. \quad (38)$$

Let's further denote the matrix obtained by taking the first $n \times n$ submatrix of U as U_n . Then, we can construct the following polynomial:

$$P(x) = \sum_{n=0}^D \frac{(-1)^n}{n!} (\det U_n) x^{D-n}, \quad (39)$$

where $\det U_0 = 1$. This polynomial is actually the characteristic polynomial of the density matrix $\hat{\rho}_A$: $P(x) = \det(xI - \hat{\rho}_A)$. Therefore, the roots of $P(x)$ are the entanglement spectrum.

D. Properties of the hyperfine structure

In the following, we will demonstrate some universal properties of the hyperfine structure $h_{n;k}$ as a quantum information quantity, including additivity, normalization, exchange symmetry, and local unitary invariance.

1. Additivity. For $i, j \in A$, $h_{n;k}(i) + h_{n;k}(j) = h_{n;k}(i \cup j)$.

Proof.

$$\begin{aligned} C_k(i) + C_k(j) &= \sum_{l \in \{i, j\}} (-i\partial_\lambda)^{k-1} \frac{\langle \exp(i\lambda \hat{N}_A) \hat{n}_l \rangle}{\langle \exp(i\lambda \hat{N}_A) \rangle} \Big|_{\lambda=0} \\ &= C_k(i \cup j) \end{aligned} \quad (40)$$

Correspondingly, $h_{n;k}(i) + h_{n;k}(j) = h_{n;k}(i \cup j)$. \square

2. Normalization. The sum of $h_{n;k}(j)$ over all sites in A equals C_k , specifically, $C_k = \sum_j h_{n;k}(j)/\beta_k(n)$.

Proof.

$$\begin{aligned}
\sum_j C_k(j) &= \sum_j (-i\partial_\lambda)^{k-1} \frac{\langle \exp(i\lambda \hat{N}_A) \hat{n}_j \rangle}{\langle \exp(i\lambda \hat{N}_A) \rangle} \Big|_{\lambda=0} \\
&= (-i\partial_\lambda)^{k-1} \frac{\langle \exp(i\lambda \hat{N}_A) \hat{N}_A \rangle}{\langle \exp(i\lambda \hat{N}_A) \rangle} \Big|_{\lambda=0} \\
&= (-i\partial_\lambda)^k \ln \langle \exp(i\lambda \hat{N}_A) \rangle \Big|_{\lambda=0} \\
&= C_k.
\end{aligned} \tag{41}$$

Correspondingly,

$$\begin{aligned}
\sum_j h_{n;k}(j) &= \sum_j \frac{1}{1-n} \sum_{k=1}^{\infty} \beta_k(n) C_k(j) \\
&= \frac{1}{1-n} \beta_k(n) \sum_{k=1}^{\infty} C_k \\
&= h_{n;k}.
\end{aligned} \tag{42}$$

□

3. Exchange symmetry. If $\hat{T} \hat{\rho}_A \hat{T}^\dagger = \hat{\rho}_A$ and \hat{T} exchanges the site i with j , then $h_{n;k}(i) = h_{n;k}(j)$.

Proof. Notice that

$$\begin{aligned}
[\hat{T}, \hat{N}_A] &= [\hat{T}, \sum_l \hat{n}_l] \\
&= [\hat{T}, \sum_{l \neq i, j} \hat{n}_l] + [\hat{T}, \hat{n}_i + \hat{n}_j] \\
&= \hat{T}(\hat{n}_i + \hat{n}_j) - (\hat{n}_i + \hat{n}_j)\hat{T}
\end{aligned} \tag{43}$$

$$= \hat{T}(\hat{n}_i + \hat{n}_j)\hat{T}^\dagger \hat{T} - (\hat{n}_i + \hat{n}_j)\hat{T} \tag{44}$$

$$= (\hat{n}_j + \hat{n}_i)\hat{T} - (\hat{n}_i + \hat{n}_j)\hat{T} \tag{45}$$

$$= 0. \tag{46}$$

Therefore, it is easy to demonstrate that

$$\begin{aligned}
\langle \exp(i\lambda \hat{N}_A) \hat{n}_j \rangle' &= \text{tr}(\hat{T} \hat{\rho}_A \hat{T}^\dagger \hat{T} \exp(i\lambda \hat{N}_A) \hat{T}^\dagger \hat{T} \hat{n}_j \hat{T}^\dagger) \\
&= \text{tr}(\hat{\rho}_A \exp(i\lambda \hat{N}_A) \hat{n}_i) \\
&= \langle \exp(i\lambda \hat{N}_A) \hat{n}_i \rangle.
\end{aligned} \tag{47}$$

Hence, under the symmetry \hat{T} , we have

$$C_k(j) = C_k(i), \tag{48}$$

which implies that

$$h_{n;k}(j) = h_{n;k}(i).$$

□

4. Local unitary Invariance. If the quantum state transforms from $|\psi\rangle$ to $|\psi'\rangle$ using a unitary transformation \hat{U}^X acting on a subset $X \subset A$, then $h_{n;k}(j \in X)$ remains the same for both states $|\psi\rangle$ and $|\psi'\rangle$.

Proof. According to the definition in Eq. (2) of the main text, the hyperfine structure for state $|\psi\rangle$ and $|\psi\rangle'$ are given by

$$h_{n;k}(j \in X) = \beta_k(n) (-i\partial_\lambda)^{k-1} \frac{\langle \exp(i\lambda \hat{N}_A) \hat{n}_{j \in X} \rangle}{\langle \exp(i\lambda \hat{N}_A) \rangle} \Big|_{\lambda=0}, \quad (49)$$

$$h'_{n;k}(j \in X) = \beta_k(n) (-i\partial_\lambda)^{k-1} \frac{\langle \exp(i\lambda \hat{N}_A) \hat{n}_{j \in X} \rangle'}{\langle \exp(i\lambda \hat{N}_A) \rangle'} \Big|_{\lambda=0}, \quad (50)$$

$$(51)$$

respectively.

The correlation functions in the numerator of the above equations are equivalent by noting that

$$\begin{aligned} \langle \exp(i\lambda \hat{N}_A) \hat{n}_{j \in X} \rangle' &= \text{tr}(\hat{\rho}'_A \exp(i\lambda \hat{N}_A) \hat{n}_{j \in X}) \\ &= \text{tr}(\hat{U}^X \hat{\rho}_A (\hat{U}^X)^\dagger \exp(i\lambda \hat{N}_A) \hat{n}_{j \in X}) \\ &= \text{tr}(\hat{\rho}_A (\hat{U}^X)^\dagger \exp(i\lambda \hat{N}_A) \hat{U}^X (\hat{U}^X)^\dagger \hat{n}_{j \in X} \hat{U}^X) \\ &= \text{tr}(\hat{\rho}_A (\hat{U}^X)^\dagger \exp(i\lambda \hat{n}_{j \in X}) \hat{U}^X I^{\bar{X}} \exp(i\lambda \hat{N}_{\bar{X}}) \hat{I}^{\bar{X}} \hat{n}_{j \in X}) \\ &= \text{tr}(\hat{\rho}_A \exp(i\lambda \hat{N}_A) \hat{n}_{j \in X}) \\ &= \langle \exp(i\lambda \hat{N}_A) \hat{n}_{j \in X} \rangle. \end{aligned} \quad (52)$$

The correlation functions in the denominator are also the same

$$\begin{aligned} \langle \exp(i\lambda \hat{N}_A) \rangle' &= \text{tr}(\hat{\rho}'_A \exp(i\lambda \hat{N}_A)) \\ &= \text{tr}(\hat{U}^X \hat{\rho}_A (\hat{U}^X)^\dagger \exp(i\lambda \hat{N}_A)) \\ &= \text{tr}(\hat{\rho}_A (\hat{U}^X)^\dagger \exp(i\lambda \hat{N}_X) \hat{U}^X I^{\bar{X}} \exp(i\lambda \hat{N}_{\bar{X}}) \hat{I}^{\bar{X}}) \\ &= \text{tr}(\hat{\rho}_A \exp(i\lambda \hat{N}_A)) \\ &= \langle \exp(i\lambda \hat{N}_A) \rangle. \end{aligned} \quad (53)$$

where $\bar{X} = A \setminus X$ and $I^{\bar{X}}$ is the identity operator that act on \bar{X} . Therefore,

$$h'_{n;k}(j \in X) = h_{n;k}(j \in X). \quad (54)$$

□

II. HYPERFINE STRUCTURE IN FERMI GAS

In this section, we will first introduce a simplified decomposition of Rényi contour in Fermi gas. Then we will discuss the hyperfine structure in (1+1)D CFT as an example, which will be useful in the next section.

A. Hyperfine structure in Fermi gas (Eq. (3)-(5) of the main text)

In the $(d+1)$ D Fermi gas, we have the following asymptotic relation

$$\frac{s_n(x)}{h_{n;2}(x)} = 1 + o(1), \quad (55)$$

which shows that the hyperfine structure $h_{n;k>2}$ are suppressed in this case.

Proof. According to the following exact relation between particle fluctuation and Rényi entropy in Fermi gas[42]

$$\frac{S_n}{C_2} = \frac{(1+n^{-1})\pi^2}{6} + o(1), \quad (56)$$

we notice that the contribution from higher cumulant ($C_{k>2}$) become negligible when compared to C_2 . Since the elements of projection operator is finite, by applying the projection operator,

$$\hat{P}_j S_n \hat{P}_j = \frac{(1+n^{-1})\pi^2}{6} \hat{P}_j C_2 \hat{P}_j + o(1) \left(\frac{(1+n^{-1})\pi^2}{6} \hat{P}_j C_2 \hat{P}_j \right), \quad (57)$$

the second part ($\sum_k h_{n;k>2}$) is also of a magnitude less than $h_{n;2}$. Hence,

$$\frac{s_n(x)}{h_{n;2}(x)} = 1 + o(1). \quad (58)$$

□

Based on the relationship between $h_{n;2}$ and the particle-number cumulant density, we can further derive an important property that relates $h_{n;2}(j)$ or $s_n(j)$ to the mutual information $I_2(A, B)$ between regions A and B . This relationship is mathematically expressed as:

$$I_2(A_1, A_2) = S(A_1) + S(A_2) - S(A_1 \cup A_2 = A) = -2 \sum_{i \in A_1, j \in A_2} [\langle \hat{n}_i \hat{n}_j \rangle - \langle \hat{n}_i \rangle \langle \hat{n}_j \rangle]. \quad (59)$$

We derive that:

$$S_A - h_{1;2}(i \in A_1) = \sum_{i \in A_1, j \in A_1} [\langle n_i n_j \rangle - \langle n_i \rangle \langle n_j \rangle] - \sum_{i \in A_1, j \in A} [\langle n_i n_j \rangle - \langle n_i \rangle \langle n_j \rangle] \quad (60)$$

$$= - \sum_{i \in A_1, j \in A_2} [\langle n_i n_j \rangle - \langle n_i \rangle \langle n_j \rangle]. \quad (61)$$

Therefore, the mutual information between regions A_1 and A_2 inside A can be reformulated as:

$$I_2(A_1, A_2) = 2(S(A_1) - h_{1;2}(i \in A_1)), \quad (62)$$

which can also be written in a continuous form as

$$I_2(A_1, A_2) = 2(S(A_1) - \int_{x \in A_1} h_{1;2}(x) dx), \quad (63)$$

where $h_{1;2}(x)$ is the hyperfine structure of region $A_1 \cup A_2 = A$.

B. Hyperfine structure in (1+1)D CFT (Eq. (6) of the main text)

Here we present an example to calculate the hyperfine structure in (1+1)D CFT, which will be useful in the section of holographic duality. In (1+1)D CFT, the leading term of the hyperfine structure $h_{n;2}$ in region A is given by

$$h_{n;2}(x) = \frac{(1+n^{-1})\pi^2}{6} \int dy [\langle \hat{n}(x) \hat{n}(y) \rangle - \langle \hat{n}(x) \rangle \langle \hat{n}(y) \rangle]. \quad (64)$$

Specifically, we consider the Euclidean action of the Dirac fermion as follows:

$$S = \frac{1}{2} \int d^2x \bar{\psi} \gamma_\mu \partial^\mu \psi, \quad (65)$$

where $\psi = (\psi_R, \psi_L)^T$. The Dirac fermions ψ_R and ψ_L have conformal weights $(1/2, 0)$ and $(0, 1/2)$, respectively. Their corresponding correlation functions are $\langle \psi_R^\dagger(z) \psi_R(\omega) \rangle = -\frac{1}{2\pi} \frac{1}{z-\omega}$, $\langle \psi_L^\dagger(\bar{z}) \psi_L(\bar{\omega}) \rangle = -\frac{1}{2\pi} \frac{1}{\bar{z}-\bar{\omega}}$.

The particle-number operator in this field is

$$\hat{n}(x) = \psi_R^\dagger(x) \psi_R(x) + \psi_L^\dagger(x) \psi_L(x). \quad (66)$$

Inserting the above expression inside Eq. (64), we have

$$\begin{aligned} \langle \hat{n}(x) \hat{n}(y) \rangle &= \langle \psi_R^\dagger(x) \psi_R(x) \psi_R^\dagger(y) \psi_R(y) \rangle + \langle \psi_L^\dagger(x) \psi_L(x) \psi_L^\dagger(y) \psi_L(y) \rangle \\ &\quad + \langle \psi_R^\dagger(x) \psi_R(x) \psi_L^\dagger(y) \psi_L(y) \rangle + \langle \psi_L^\dagger(x) \psi_L(x) \psi_R^\dagger(y) \psi_R(y) \rangle, \end{aligned} \quad (67)$$

and

$$\begin{aligned} \langle \hat{n}(x) \rangle \langle \hat{n}(y) \rangle &= \langle \psi_R^\dagger(x) \psi_R(x) \rangle \langle \psi_R^\dagger(y) \psi_R(y) \rangle + \langle \psi_R^\dagger(x) \psi_R(x) \rangle \langle \psi_L^\dagger(y) \psi_L(y) \rangle \\ &+ \langle \psi_L^\dagger(x) \psi_L(x) \rangle \langle \psi_R^\dagger(y) \psi_R(y) \rangle + \langle \psi_L^\dagger(x) \psi_L(x) \rangle \langle \psi_L^\dagger(y) \psi_L(y) \rangle. \end{aligned} \quad (68)$$

Based on Wick's theorem and the chiral symmetry condition $\langle \psi_R^\dagger \psi_L \rangle = \langle \psi_L^\dagger \psi_R \rangle = 0$, we have

$$\langle \hat{n}(x) \hat{n}(y) \rangle - \langle \hat{n}(x) \rangle \langle \hat{n}(y) \rangle = - \langle \psi_R^\dagger(x) \psi_R(y) \rangle \langle \psi_R^\dagger(y) \psi_R(x) \rangle - \langle \psi_L^\dagger(x) \psi_L(y) \rangle \langle \psi_L^\dagger(y) \psi_L(x) \rangle \quad (69)$$

$$= \frac{1}{2\pi^2} \frac{1}{(x-y)^2}. \quad (70)$$

Therefore, the leading hyperfine structure $h_{n;2}$ can be written as

$$\begin{aligned} h_{n;2}(x) &= \frac{(1+n^{-1})\pi^2}{6} \int_{-R+\epsilon}^{R-\epsilon} \frac{1}{2\pi^2} \frac{1}{(x-y)^2} dy \\ &= \frac{(1+n^{-1})}{12} \left(\frac{1}{R-x} + \frac{1}{R+x} \right). \end{aligned} \quad (71)$$

By integrating $s_n(x)$ over A , we obtain the Rényi entropy as $S_n = \int_{-R+\epsilon}^{R-\epsilon} dx s_n(x) \approx [(1+n^{-1})/6] \ln \frac{2R}{\epsilon}$. Comparing the known equality $S_n = [(1+n^{-1})c/6] \ln \frac{2R}{\epsilon}$, we end up with the value of the central charge $c = 1$, which agrees with the known fact of Dirac fermions models.

Here, we observe that the contour function in a Fermi gas, given by $s_n \approx h_{n;2} = \frac{c}{12}(1+n^{-1}) \left(\frac{1}{R-x} + \frac{1}{R+x} \right)$, aligns with the contour function with conformal symmetry as defined in Ref. [21]. Remarkably, this expression holds true regardless of the presence of interaction or the specifics of the Hamiltonian.

Consequently, it is natural to ask whether the relationship between the contour function and the density of the particle-number cumulant still persists in general interacting (1+1)D CFT. In the following, we will demonstrate that this relationship does indeed hold, up to a constant. Specifically, we find that

$$\frac{s_n(x)}{c_2(x)} = \text{constant} + o(1). \quad (72)$$

Proof. According to the definition of the density of particle-number cumulant, we have the following expression

$$c_2(i) = \sum_{j \in A} [\langle n_i n_j \rangle - \langle n_i \rangle \langle n_j \rangle]. \quad (73)$$

By dividing the subsystem A into A_1, A_2, A_3 . It is easy to check the linear combination relation between the density of particle-number cumulant contributed from region A_2 and the particle-number cumulant

$$c_2(A_2) = \frac{1}{2} (C_2(A_1 \cup A_2) + C_2(A_2 \cup A_3) - C_2(A_1) - C_2(A_3)). \quad (74)$$

The left side of the equation is

$$c_2(A_2) = \sum_{i \in A_2} \sum_{j \in A} [\langle n_i n_j \rangle - \langle n_i \rangle \langle n_j \rangle], \quad (75)$$

which is the same as the right side of the equation.

The continuous form of Eq. (74) in 1+1d CFT is

$$c_2(x) = \frac{1}{2} \left(\frac{\partial C_2(x_1, x)}{\partial x} - \frac{\partial C_2(x, x_2)}{\partial x} \right), \quad (76)$$

where x_1, x_2 are the coordinates of the boundary of region A , and $C(x_1, x)$ is a function of coordinates of the boundary x_1, x .

In (1+1)D CFT, the particle-number fluctuation is [18]

$$C_2(A) = \frac{g}{\pi^2} \ln \left(\frac{2R}{\epsilon} \right), \quad (77)$$

where the prefactor g can be fixed by considering the conserved charge and ε is the cutoff.

Based on Eq. (76) and Eq. (77), we have

$$c_2(x) = \frac{g}{2\pi^2} \left(\frac{1}{R-x} + \frac{1}{R+x} \right). \quad (78)$$

Therefore, the ratio between $s_2(x)$ and $c_2(x)$ is a constant

$$\frac{s_n(x)}{c_2(x)} = \frac{\frac{c}{12}(1+n^{-1})\left(\frac{1}{R-x} + \frac{1}{R+x}\right)}{\frac{g}{2\pi^2}\left(\frac{1}{R-x} + \frac{1}{R+x}\right)} = \frac{\pi^2 c(1+n^{-1})}{6g}. \quad (79)$$

This relation can be generalized to $h_{h;2}$ and $\tilde{h}_{n;2}$ in CFT directly. \square

III. HYPERFINE STRUCTURE IN ADS/CFT CORRESPONDENCE

In this section, we will introduce the holographic duality of the hyperfine structure in the context of $\text{AdS}_3/\text{CFT}_2$.

A. Refined Rényi entropy and its hyperfine structure (Eq. (7) of the main text)

To explore the holographic duality of the Rényi contour s_n , it is advantageous to utilize the concept of refined Rényi entropy, defined as $\tilde{S}_n \equiv n^2 \partial_n \left(\frac{n-1}{n} S_n \right)$. The contour function and the hyperfine structure can be extended to the refined Rényi entropy as indicated in Eq. (7) of the main text.

In the following, we will first establish that the refined Rényi entropy represents the entanglement entropy of a new density matrix, $\tilde{\rho}_A = \frac{(\hat{\rho}_A)^n}{\text{tr}(\hat{\rho}_A)^n}$. Subsequently, we will derive the relationship described in Eq. (7) of the main text.

Proof. Considering a pure state $|\psi\rangle$ in Hilbert space $\mathcal{H} = \mathcal{H}_A \otimes \mathcal{H}_B$, the Schmidt decomposition is as follows,

$$|\psi\rangle = \sum_q a_q |\psi_A^q\rangle \otimes |\psi_B^q\rangle, \quad (80)$$

where $\{|\psi_A^q\rangle\}$ is an orthogonal basis for \mathcal{H}_A and $\{|\psi_B^q\rangle\}$ is an orthogonal basis for \mathcal{H}_B and the Schmidt numbers sum up to one, $\sum_q a_q^2 = 1$. The reduced density matrix of region A is

$$\hat{\rho}_A = \sum_q a_q^2 (|\psi_A^q\rangle \langle \psi_A^q|). \quad (81)$$

The refined Rényi contour $\tilde{S}_n(\hat{\rho}_A)$ can be written as the von Neumann entropy of a new density matrix $\tilde{\rho}_A = \frac{\hat{\rho}_A^n}{\text{tr} \hat{\rho}_A^n}$,

$$\begin{aligned} \tilde{S}_n(\hat{\rho}_A) &= -n^2 \partial_n \left(\frac{1}{n} \ln \text{tr} \hat{\rho}_A^n \right) \\ &= \ln \text{tr} \hat{\rho}_A^n - n \partial_n \ln \text{tr} \hat{\rho}_A^n \\ &= \ln \text{tr} \hat{\rho}_A^n - \frac{\text{tr}(\hat{\rho}_A^n \ln \hat{\rho}_A^n)}{\text{tr}(\hat{\rho}_A^n)} \\ &= -\text{tr} \left(\frac{\hat{\rho}_A^n}{\text{tr} \hat{\rho}_A^n} \right) \ln \left(\frac{\hat{\rho}_A^n}{\text{tr} \hat{\rho}_A^n} \right) \\ &= S \left(\frac{\hat{\rho}_A^n}{\alpha_n} \right) \end{aligned} \quad (82)$$

where we denote $\alpha_n = \text{tr} \hat{\rho}_A^n$. \square

Here we further discuss the entanglement Hamiltonian of the n -replica reduced density matrix $\tilde{\rho}_A = \frac{(\hat{\rho}_A)^n}{\text{tr}(\hat{\rho}_A)^n}$. The original density density matrix is

$$\begin{aligned}\hat{\rho}_A &= \sum_p a_p^2 |\psi_A^p\rangle\langle\psi_A^p| \\ &= \frac{e^{-\hat{K}_A}}{Z},\end{aligned}\tag{83}$$

where the corresponding entanglement Hamiltonian is

$$\hat{K}_A = \sum_p -\ln a_p^2 |\psi_A^p\rangle\langle\psi_A^p|,\tag{84}$$

and Z is the normalization constant. The density matrix is a Gibbs state with temperature $T = 1$. The n -replica density matrix is defined as

$$\begin{aligned}\tilde{\rho}_A^{(n)} &\equiv \sum_p \frac{a_p^{2n}}{\alpha_n} |\psi_A^p\rangle\langle\psi_A^p| \\ &= \frac{e^{-\hat{K}_A^{(n)}}}{Z^{(n)}},\end{aligned}\tag{85}$$

where $\alpha_n = \sum_q a_q^{2n}$ and

$$\hat{K}_A^{(n)} = n\hat{K}_A.\tag{86}$$

Here, $Z^{(n)}$ represents a new normalization constant, and the temperature of the Gibbs state is now set to $T = \frac{1}{n}$. It is important to emphasize that the two entanglement Hamiltonians commute, $[\hat{K}_A^{(n)}, \hat{K}_A] = 0$, yet their spectra differ.

In the following, we will present two different ways to derive the Eq. (7) of the main text.

Firstly, Eq. (7) of the main text can be easily determined from the definition of the refined Rényi contour in Eq. (6) of the main text in CFT.

Secondly, we can use the analytical form of entanglement Hamiltonian \hat{K}_A and $\hat{K}_A^{(n)}$ to verify the Eq. (7) of the main text. In the Fermi gas, the entanglement Hamiltonian takes an analytical form resembling the following tridiagonal matrix, as described in Ref. [43]:

$$K = \begin{pmatrix} d_1 & t_1 & & & \\ t_1 & d_2 & t_2 & & \\ & t_2 & d_3 & & \\ & & & \ddots & t_{\mathcal{N}_A-1} \\ & & & t_{\mathcal{N}_A-1} & d_{\mathcal{N}_A} \end{pmatrix},$$

with the matrix elements defined as:

$$t_i = \frac{i}{\mathcal{N}_A} \left(1 - \frac{i}{\mathcal{N}_A}\right), \quad d_i = -2 \cos q_F \frac{2i-1}{2\mathcal{N}_A} \left(1 - \frac{2i-1}{2\mathcal{N}_A}\right),\tag{87}$$

where $q_F = \frac{\pi}{2}$ represents the Fermi momentum at the critical point. Based on Eq. (86) and Eq. (87) as well as exact diagonalization, it is easy to confirm that the refined Rényi contour $\tilde{s}_n(x)$ derived from nT and the Rényi contour derived from T satisfy the relationship:

$$\tilde{s}_n(x) = \frac{1}{n} s_1(x),\tag{88}$$

which aligns with Eq. (7) of the main text.

B. Rindler transformation in AdS₃/CFT₂

In the following, we will introduce the holographic duality of hyperfine structure $h_{n,2}$ using Rindler transformation. The basic idea of Rindler transformation is to convert the entanglement entropy of a region into the thermal entropy of another region

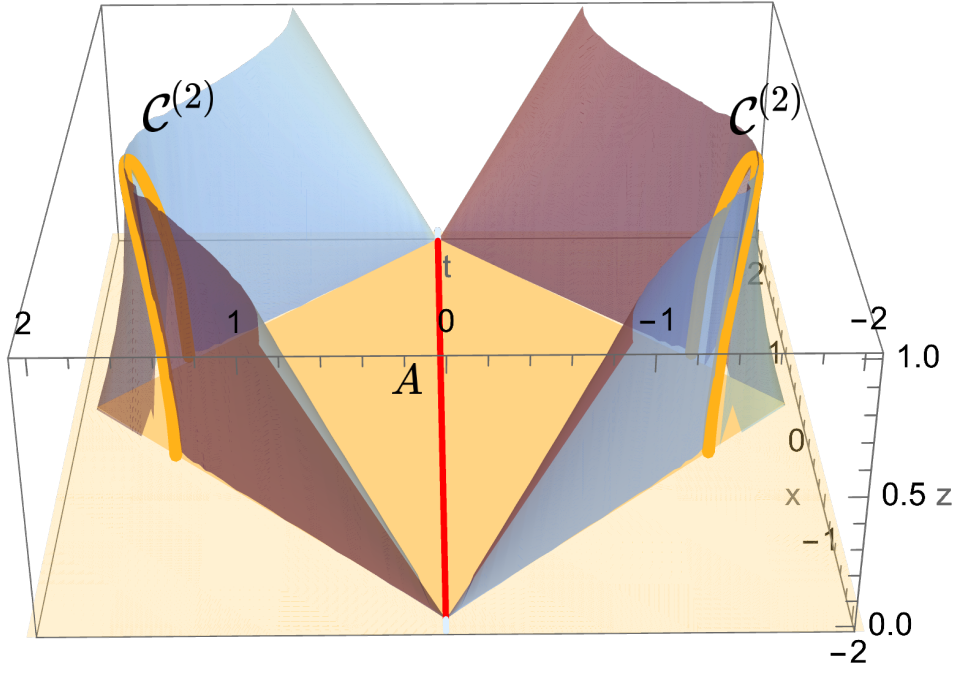


FIG. 4. The red line represents subregion A . The two transparent surfaces are $\mathcal{N}_{\pm}^{(n)}$ with $n = 2$, and their intersections are highlighted by yellow lines, which correspond to the extremal surfaces for $n = 2$. These extremal surfaces, denoted $\mathcal{C}^{(2)}$, are anchored at and traverse along the entangling surface. They also exhibit tension and conical defects that cause backreactions to the bulk geometry, such as the discontinuity in $\mathcal{N}_{\pm}^{(n)}$. We set $l_u = l_v = 2$ in the figure.

which can be mapped to the horizon entropy of a hyperbolic black hole. It turns out that the horizon corresponds to the null hypersurfaces in the original Poincaré AdS spacetime. The intersection of null hypersurfaces $\mathcal{N}_{\pm}^{(1)}$ in Poincaré AdS₃ forms the extremal surface \mathcal{E}_A . Furthermore, the intersection of the n -dependent null hypersurfaces $\mathcal{N}_{\pm}^{(n)}$ in the n -dependent Poincaré AdS₃ represents the holographic dual of \tilde{S}_n .

Suppose A is the interval on the infinite line in the ground state in (1+1)D CFT, which is a straight interval with the two boundaries on $(u_1, v_1) = (-\frac{l_u}{2}, -\frac{l_v}{2})$ and $(u_2, v_2) = (\frac{l_u}{2}, \frac{l_v}{2})$ in the Poincaré AdS₃ with the metric

$$ds^2 = 2rdu dv + \frac{dr^2}{4r^2}. \quad (89)$$

Here we consider the AdS radius $l = 1$. We can go back to the original Poincaré AdS₃ $ds^2 = \frac{dx^2 + dz^2 - dt^2}{z^2}$ by setting

$$u = \frac{x+t}{2}, \quad v = \frac{x-t}{2}, \quad r = \frac{2}{z^2}. \quad (90)$$

In the original Poincaré AdS₃, the two boundaries of subregion A are $(x_1, t_1) = (-R, 0)$ and $(x_2, t_2) = (R, 0)$, where $R = \frac{l_u + l_v}{2}$. The causal development of A is the diamond-shape subregion

$$-\frac{l_u}{2} \leq u \leq \frac{l_u}{2}, \quad -\frac{l_v}{2} \leq v \leq \frac{l_v}{2}. \quad (91)$$

In the case of refined Rényi entropy, we consider the following metric of the n -dependent Poincaré AdS₃ [29]

$$ds^2 = \rho^2 d\tilde{y}^2 + (\rho^2 - \rho_h^2) d\tilde{\tau}^2 + \frac{d\rho^2}{\rho^2 - \rho_h^2}, \quad (92)$$

with $\rho_h = \frac{1}{n}$. This n -dependent AdS₃ can also be written as

$$ds^2 = \frac{d\tilde{r}^2}{4(\tilde{r}+1)(\tilde{r}+1-2\rho_h^2)} + \rho_h^2 d\tilde{u}^2 + \rho_h^2 d\tilde{v}^2 + 2\left(\frac{\tilde{r}+1}{\rho_h^2} - 1\right)\rho_h^2 d\tilde{u}d\tilde{v},$$

by setting

$$\tilde{r} + 1 = 2\rho^2, \tilde{u} = \frac{\tilde{y} + \tau}{2}, \tilde{v} = \frac{\tilde{y} - \tau}{2}, \tau = i\tilde{\tau}. \quad (93)$$

The above form can be easily transformed into the Rindler AdS₃

$$ds^2 = du^{*2} + r^{*2} du^* dv^* + dv^{*2} + \frac{dr^{*2}}{4(r^{*2} - 1)}, \quad (94)$$

using

$$u^* = \rho_h \tilde{u}, v^* = \rho_h \tilde{v}, r^* = \frac{\tilde{r} + 1}{\rho_h^2} - 1. \quad (95)$$

Therefore, the Rindler transformation from coordinate (u, v, r) to (u^*, v^*, r^*) is

$$\begin{aligned} u^* &= \frac{\rho_h}{4} \ln\left(\frac{4(rv(l_u + 2u) + 1)^2 - l_v^2 2r^2(l_u + 2u)^2}{4(rv(l_u - 2u) - 1)^2 - l_v^2 r^2(l_u - 2u)^2}\right), \\ v^* &= \frac{\rho_h}{4} \ln\left(\frac{l_u^2 r^2(l_v + 2v)^2 - 4(l_v r u + 2r u v + 1)^2}{l_u^2 r^2(l_v - 2v)^2 - 4(-l_v r u + 2r u v + 1)^2}\right), \\ (r^* + 1)\rho_h^2 - 1 &= \frac{r^2(l_u^2(l_v^2 - 4v^2) - 4l_v^2 u^2) + 4(2r u v + 1)^2}{4l_u l_v r}. \end{aligned}$$

By setting $r^* = 1$, the horizon of the n -Rindler AdS₃ maps to the two null hypersurfaces $\mathcal{N}_{\pm}^{(n)}$ in the original space (u, v, r)

$$\mathcal{N}_+^{(n)} : r = \frac{-2n^2}{l_u^2(n^2 - 2) + 4n^2 uv + 2l_u \sqrt{l_u^2(1 - n^2) - 4n^2 uv + n^4(u + v)^2}}, \quad (96)$$

$$\mathcal{N}_-^{(n)} : r = \frac{-2n^2}{l_u^2(n^2 - 2) + 4n^2 uv - 2l_u \sqrt{l_u^2(1 - n^2) - 4n^2 uv + n^4(u + v)^2}}. \quad (97)$$

As we can see in the Fig. 1(c) of the main text, the intersection of the null hypersurfaces $\mathcal{N}_{\pm}^{(1)}$ provides the RT surface \mathcal{E}_A . The entanglement wedge is defined as the bulk domain of dependence bounded by A and the RT surface \mathcal{E}_A . Within the entanglement wedge, the bulk operators can be reconstructed from the boundary CFT, which is the well-known subregion-subregion duality in holographic duality [31].

The intersection of $\mathcal{N}_{\pm}^{(n)}$ provides the extremal surface \tilde{S}_n within the original coordinates (x, t, z) , as depicted in Fig. 4. The extremal surfaces, denoted as $\mathcal{C}^{(n)}$, for $n > 1$ differ markedly from the $n = 1$ RT surface. It is noteworthy that the extremal surfaces $\mathcal{C}^{(n)}$ are inclined and exhibit a conical defect, manifesting as discontinuous regions in the null hypersurface $\mathcal{N}_{\pm}^{(n)}$. However, this singularity disappears when $n = 1$.

Interestingly, $\mathcal{C}^{(n)}$ extend beyond the entanglement wedge, which implies that they cannot be connected to \mathcal{E}_A through time unitary evolution. This aligns with the principle that a unitary transformation does not modify the entanglement spectrum of a density matrix. Therefore, we can further define the Rényi entanglement wedge enclosed by $\mathcal{C}^{(n)}$. Intriguingly, this observation extends the bulk reconstruction based on the entanglement wedge [32, 33], which allows the reconstruction of bulk local operators outside the entanglement wedge.

Moreover, as is shown in Fig. 5, with the help of the hyperfine structure we introduced, we can find out a finer description for the subregion-subregion duality in entanglement wedge and Rényi entanglement wedge. We can use the planes that link the boundary sites with the extremal surfaces $\mathcal{C}^{(n)}$ to slice the extremal surface according to the contour distribution. Each segment derived from the extremal surface represents the holographic dual of the hyperfine structure. Thus, the holographic description of Rényi entropy is refined into the duality between the boundary density-density correlator and the segment of bulk extremal surface. This finer correspondence indicates that a bulk local operator can be reconstructed by CFT operators in a segment of the subregion on the boundary.

IV. HYPERFINE STRUCTURE IN LATTICE FERMION MODELS

In Fermi gas systems, higher ranks of the hyperfine structure are suppressed. However, in more general cases, we observe a variety of parameter regions where $h_{n;k>2}$ contributes to both the fine structure and entropy. In the forthcoming sections, we will

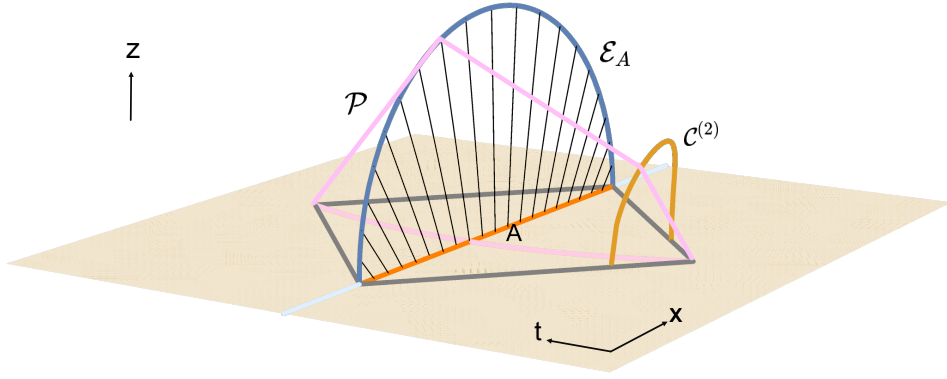


FIG. 5. Slice the extremal surfaces according to the distribution of the hyperfine structure using the pink plane.

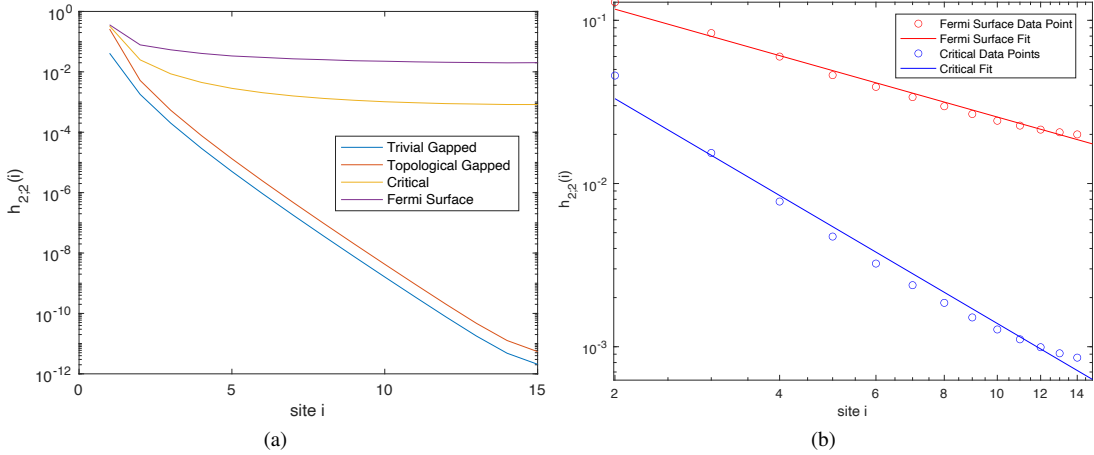


FIG. 6. The cross section of the hyperfine structure $h_{2,2}(x)$ in the four parameter regions. From Fig.(a) we can find that in the cases of both trivial gapped and topological gapped, $h_{2,2}(x)$ decrease exponentially from the boundary to the bulk. From both (a) and (b) we can see that the $h_{2,2}(x)$ of critical and Fermi surface decrease in a power law.

explore the behavior of all ranks of the hyperfine structure in lattice fermion models. Initially, we will examine the distribution function of $h_{n,2}$ across different parameter regions. Subsequently, we will demonstrate the emergent scaling law of normalized $h_{n,k}(m; k_x = 0, \pi)$ in the presence of topological edge states.

A. Distribution function of $h_{n,2}$ in various parameter regions

As illustrated in Fig. 2 in the main text, the behavior of the leading component $h_{n,2}$ is similar across different across parameter regions: it predominantly localizes on the boundary and exhibits a decay from the boundary towards the center. To further explore the distribution function of $h_{n,2}$ across various parameter regions, we present a cross-sectional analysis of the hyperfine structure $h_{n,2}$ in Fig. 6. For clarity, we set $n = 2$. As shown in Fig. 6(a), it is apparent that in both trivially gapped and topologically gapped scenarios, $h_{n,2}$ exhibit an exponential decrease. In contrast, at critical points and along Fermi surfaces, $h_{n,2}$ decreases following a power-law decay, which is notably slower than the exponential decline.

Furthermore, it is noteworthy that the power-law exponents at critical points and Fermi surfaces are distinct. The decay of $h_{n,2}$ at critical points is faster than that at Fermi surfaces. Despite the similarities in scaling behavior of entanglement entropy between critical points and trivially gapped cases, the distribution functions of the hyperfine structure $h_{n,2}$ exhibit marked differences.

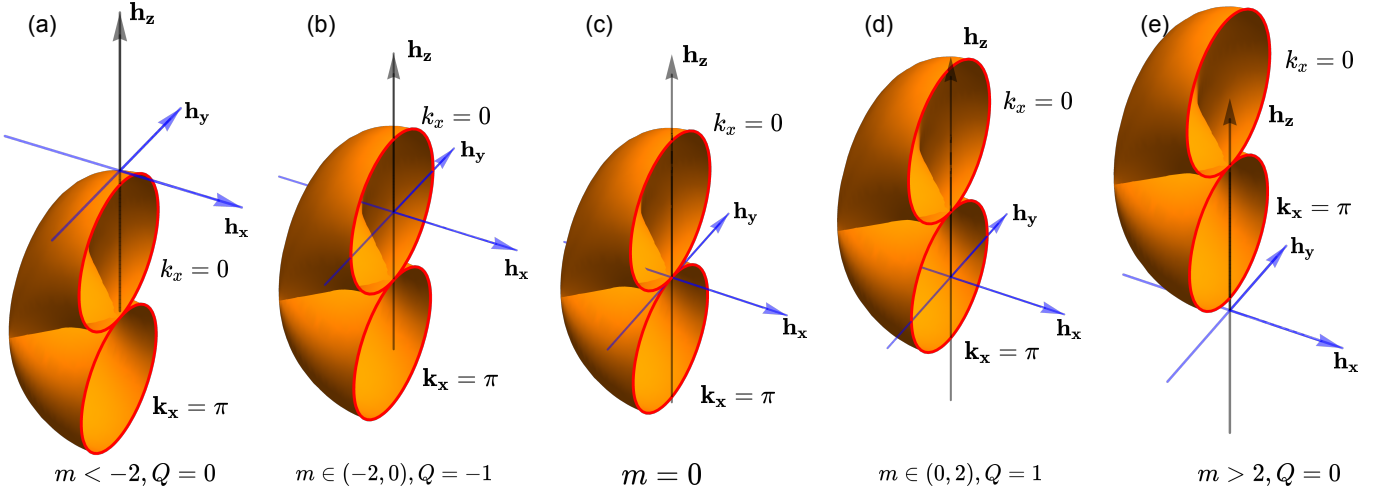


FIG. 7. The torus $\mathbf{h}(\mathbf{k})$ of the Chern insulator for different values of m . In (a), (c) and (e), the torus do not contain the origin hence Chern number $Q=0$. In (b), the red circle with $k_x = 0$ encloses the origin, meaning that there are zero-energy edge states at this k_x . At $k_x = \pi$, the red loop lies in the plane of the origin without containing it, indicating no edge state at $k_x = \pi$. (d) is similar to (b) but has zero-energy edge state at $k_x = \pi$.

B. Edge states of Chern insulator

In this subsection, we will demonstrate the emergent scaling law of normalized $h_{n;k}(m; k_x = 0, \pi)$ shown in Fig. 3 in the presence of topological edge states. Initially, we establish the link between the bulk Chern number and the zero-energy modes in the Chern insulator model, denoted as $\hat{\mathcal{H}} = \sum_{\mathbf{k}} \hat{c}_{\mathbf{k}}^\dagger h(\mathbf{k}) \cdot \sigma \hat{c}_{\mathbf{k}}$ with $h(\mathbf{k}) = (\sin k_x, \sin k_y, m + \cos k_x + \cos k_y)$, where σ is the vector of Pauli matrices. By considering an open boundary along the y-axis and a periodic boundary along the x-axis, we classify different quantum states using the quantum number k_x . We demonstrate that within the topological interval $m \in (-2, 0)$, the zero-energy edge mode corresponds to $k_x = 0$, whereas for $m \in (0, 2)$, it aligns with $k_x = \pi$. Here we only present a torus argument as shown in Fig. 7 with the rigorous proof demonstrated in Ref. [44]. The critical loops of fixed k_x are highlighted in red. In Fig. 7(b) and (d), since the Chern number $Q \neq 0$, the torus wraps the origin and it is always possible to find two loops that are coplanar with the origin, one of which encloses the origin and the other does not. Specifically, at $k_x = \pi$ in Fig. 7(d), the loop that is coplanar with and encircles the origin signifies the presence of zero-energy edge states at this k_y value.

According to Refs. [45, 46], it has been identified that in specific topological zones, zero-energy edge states at $k_x = 0$ for $m \in (-2, 0)$ and at $k_x = \pi$ for $m \in (0, 2)$ correspond to entanglement modes with a fractional value of $\frac{1}{2}$.

In the topological region where $m \in (-2, 0)$, we derive the following expression:

$$\begin{aligned}
 h_{n;k}(m; k_x = 0) &= \beta_k(n) C_k(m; j \in \partial A, k_x = 0) \\
 &\approx \beta_k(n) C_k(m; k_x = 0) \\
 &= \beta_k(n) (-i\partial_\lambda)^k \ln \det(1 + M(m; k_x = 0) \exp(i\lambda)) \Big|_{\lambda=0} \\
 &= \beta_k(n) \text{tr} [(-i\partial_\lambda)^k \ln(1 + M(m; k_x = 0) \exp(i\lambda))] \Big|_{\lambda=0} \\
 &\approx \beta_k(n) (-i\partial_\lambda)^k \ln \left(1 + \frac{1}{2} \exp(i\lambda)\right) \Big|_{\lambda=0}.
 \end{aligned} \tag{98}$$

This analysis establishes a scaling law applicable across different values of k :

$$\frac{h_{n;k}(m \in (-2, 0); k_x = 0)}{\max h_{n;k}(m \in (-2, 0); k_x = 0)} = \frac{h_{n;k}(m \in (0, 2); k_x = \pi)}{\max h_{n;k}(m \in (0, 2); k_x = \pi)} \approx 1. \tag{99}$$

This scaling law is also valid in the topological domain of $m \in (0, 2)$, demonstrating a consistent pattern across the specified ranges.

V. EXPERIMENT

In this section, we will first introduce an alternative experiment protocol based on quantum point contact to measure the hyperfine structure. Then we will introduce the relationship between the entanglement of pre-measurement states and post-measurement states through the hyperfine structure.

A. Protocol based on quantum point contact

In this part, we will provide a promising experimental setup to measure the hyperfine structure of the entanglement. Before the introduction of the experimental proposal, we will firstly demonstrate the Eq. (101), which is useful for the experiment realization.

Using the equation shown in Eq. (32), which is $\langle e^{i\lambda(\sum_{i=1}^{\mathcal{N}_A} c_i^\dagger c_i)} c_l^\dagger c_l \rangle = e^{i\lambda} \langle e^{i\lambda(\sum_{i=1, i \neq l}^{\mathcal{N}_A} c_i^\dagger c_i)} c_l^\dagger c_l \rangle$, $G(\lambda, j)$ defined in Eq. (26) can be simplified as

$$\begin{aligned}
G(\lambda, j) &= \left\langle \left(\prod_{i=1, i \neq j}^{\mathcal{N}_A} [1 + (e^{i\lambda} - 1) \hat{c}_i^\dagger \hat{c}_i] \right) e^{i\lambda} \hat{c}_j^\dagger \hat{c}_j \right\rangle \\
&= \left\langle \left(\prod_{i=1, i \neq j}^{\mathcal{N}_A} [1 + (e^{i\lambda} - 1) \hat{c}_i^\dagger \hat{c}_i] \right) [1 + (e^{i\lambda} - 1) \hat{c}_j^\dagger \hat{c}_j] \right\rangle - \left\langle \prod_{i=1, i \neq j}^{\mathcal{N}_A} [1 + (e^{i\lambda} - 1) \hat{c}_i^\dagger \hat{c}_i] \right\rangle \\
&\quad + \left\langle \left(\prod_{i=1, i \neq j}^{\mathcal{N}_A} [1 + (e^{i\lambda} - 1) \hat{c}_i^\dagger \hat{c}_i] \right) \hat{c}_j^\dagger \hat{c}_j \right\rangle \\
&= \left\langle \prod_{i=1}^{\mathcal{N}_A} [1 + (e^{i\lambda} - 1) \hat{c}_i^\dagger \hat{c}_i] \right\rangle - \left\langle \prod_{i=1, i \neq j}^{\mathcal{N}_A} [1 + (e^{i\lambda} - 1) \hat{c}_i^\dagger \hat{c}_i] \right\rangle \\
&\quad + \left\langle \left(\prod_{i=1, i \neq j}^{\mathcal{N}_A} [1 + (e^{i\lambda} - 1) \hat{c}_i^\dagger \hat{c}_i] \right) \hat{c}_j^\dagger \hat{c}_j \right\rangle \\
&= \chi(\lambda, \mathcal{N}_A) - \chi(\lambda, \mathcal{N}_A - 1; j) + \left\langle \left(\prod_{i=1, i \neq j}^{\mathcal{N}_A} [1 + (e^{i\lambda} - 1) \hat{c}_i^\dagger \hat{c}_i] \right) \hat{c}_j^\dagger \hat{c}_j \right\rangle,
\end{aligned}$$

where $\chi(\lambda, \mathcal{N}_A - 1; j)$ is the cumulant generating function of region A' with the \mathcal{N}_A sites, which is a region obtained by removing site j from the original region A . Hence, we can obtain the following relation

$$\begin{aligned}
G(\lambda, j) &= \left\langle \left(\prod_{i=1, i \neq j}^{\mathcal{N}_A} [1 + (e^{i\lambda} - 1) \hat{c}_i^\dagger \hat{c}_i] \right) e^{i\lambda} \hat{c}_j^\dagger \hat{c}_j \right\rangle \\
&= [\chi(\lambda, \mathcal{N}_A) - \chi(\lambda, \mathcal{N}_A'; j)] \frac{e^{i\lambda}}{e^{i\lambda} - 1}.
\end{aligned} \tag{100}$$

Therefore, the density of particle-number cumulant in Eq. (25) can be simplified as a function of two different cumulant generating functions with different ways of partition.

$$C_k(l) = (-i\partial_\lambda)^{k-1} \left\{ \frac{[\chi(\lambda, \mathcal{N}_A) - \chi(\lambda, \mathcal{N}_A - 1; l)]}{\chi(\lambda, \mathcal{N}_A)} \frac{e^{i\lambda}}{e^{i\lambda} - 1} \right\} \Big|_{\lambda=0}. \tag{101}$$

The key observation is that the cumulant generating function $\chi(\lambda, \mathcal{N}_A)$ and $\chi(\lambda, \mathcal{N}_A - 1; l)$ can be obtained by measuring the cumulants in specific partition configurations based on the quantum point contact(QPC) method. $\chi(\lambda, \mathcal{N}_A)$ corresponds to the bi-partition shown in the left figure of Fig. 8 and $\chi(\lambda, \mathcal{N}_A - 1; l)$ corresponds to the partition arrangement illustrated in the right figure of Fig. 8, where A and B are not simply connected spaces. The subregion A in the right figure corresponds to the outcome of removing site j from the left subregion A , with site j now becoming part of subregion B . To mitigate interference within the different parts of A/B , we establish additional channels connecting them, positioned above and below the setting.

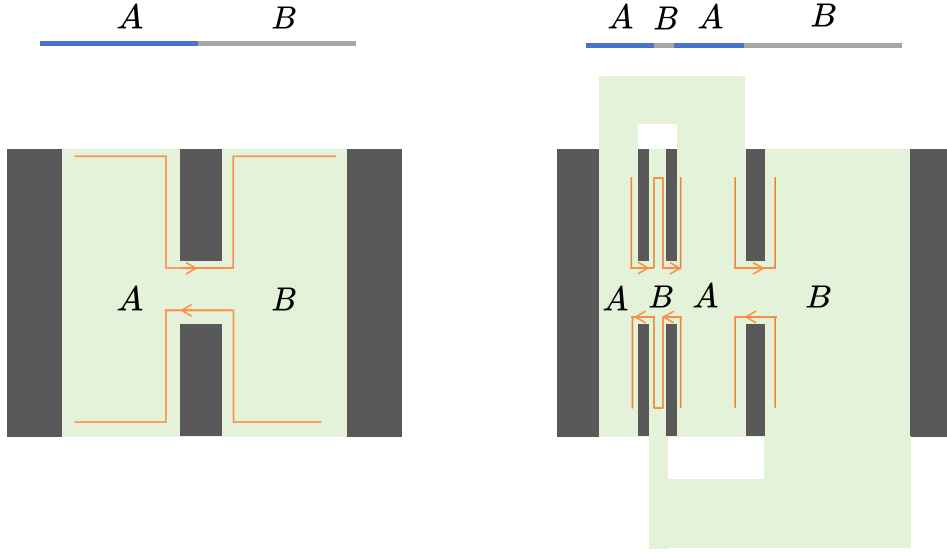


FIG. 8. Quantum Point Contact settings of two types of partition. The left figure corresponds to the bi-partition of $\chi(\lambda, \mathcal{N}_A)$ and the right one corresponds to the partition way of $\chi(\lambda, \mathcal{N}_{A'}; l)$.

Based on these QPC settings, we can reconstruct the cumulant generating function by measuring the former a few dominant cumulants. To be more precise, considering that the Taylor expansion $\chi(\lambda, \mathcal{N}_A) = \sum_{k=0}^{\infty} C_k \frac{\lambda^k}{k!}$ centering at $\lambda = 0$, we can reasonably approximate $\chi(\lambda, \mathcal{N}_A)$ by determining the first a few terms of the cumulants while the higher-order terms make negligible contributions. These cumulants are experimentally observable in the scheme shown in the left figure of Fig. 8 as demonstrated in previous studies [17, 47]. These methods can also naturally be applied to the second scheme shown in the right figure of Fig. 8. Hence, $\chi(\lambda, \mathcal{N}_A)$ and $\chi(\lambda, \mathcal{N}_A - 1; l)$ can be approximately determined experimentally, which means that $C_k(l)$ in Eq. (101) can also be obtained using previous experiment methods.

B. Pre- and Post- measurement states

The hyperfine structure unveils the relationship between the entanglement of pre-measurement states and post-measurement state sand provides the cumulant decomposition of the post measurement states under the position projection operator.

Proof. To demonstrate these points, it is convenient to replace the L creation and annihilation operators by $2L$ Majorana operators

$$\psi_{i,1} = \frac{c_i + c_i^\dagger}{\sqrt{2}}, \psi_{i,2} = \frac{c_i - c_i^\dagger}{i\sqrt{2}}. \quad (102)$$

The single-particle density matrix of free-fermion system is defined as

$$\hat{\varrho}_{ij;\mu,\nu} = \langle \psi_{i,\mu} \psi_{j,\nu} \rangle, \quad (103)$$

which is exactly the correlation matrix M in the Majorana Basis. It can be diagonalized as

$$\hat{\varrho} = O \left(\bigoplus_{k=1}^L \begin{bmatrix} \eta_k & 0 \\ 0 & 1 - \eta_k \end{bmatrix} \right) O^\dagger, \quad (104)$$

where $\{\eta_k\} \cup \{1 - \eta_k\}$ are the eigenvalues of $\hat{\varrho}$ and O is the diagonalization matrix.

Suppose we perform a projective measurement on the system described by the position projectors $\hat{P}_i = |i\rangle\langle i|$. Outcome i occurs with probability

$$p(i) = \text{tr}(\hat{P}_i \hat{\varrho}). \quad (105)$$

The quantum state after measurement is[48]

$$\tilde{\varrho} = \frac{\hat{P}_i \hat{\varrho} \hat{P}_i}{p_i}. \quad (106)$$

It is straightforward to verify that the entanglement entropy of the system post-measurement is directly linked to the entanglement contour of the pre-measurement state $\hat{\varrho}$,

$$\begin{aligned} S_1(p_i \tilde{\varrho}) &= -\text{tr}(p_i \tilde{\varrho} \ln p_i \tilde{\varrho}) \\ &= \text{tr}(f(\hat{P}_i \hat{\varrho} \hat{P}_i)), f(x) = -x \ln x \\ &= \text{tr}(f(\hat{P}_i \hat{\varrho} \hat{P}_i)) \\ &= \text{tr}(\hat{P}_i f(\hat{\varrho})) \\ &= s_1(i). \end{aligned} \quad (107)$$

Here we notice that $\hat{P}_i = \hat{P}_i^\dagger$, then $\hat{P}_i \hat{\varrho} \hat{P}_i$ can be diagonalized to Γ_i as

$$\begin{aligned} Q \hat{P}_i \hat{\varrho} \hat{P}_i Q^\dagger &= Q \hat{P}_i O \Gamma O^\dagger \hat{P}_i Q^\dagger \\ &= U \Gamma_i U^\dagger, \end{aligned} \quad (108)$$

where $U = Q \hat{P}_i O$ and the only non-zero eigenvalues of Γ_i are $\{\eta_i, 1 - \eta_i\}$.

The relation can also be generalized to Rényi entropy and Rényi contour of the pre-measurement state $\hat{\varrho}$ as

$$S_n(p_i \tilde{\varrho}) = s_n(i) = \sum_k h_{n;k}(j). \quad (109)$$

Hence, the hyperfine structure unveils the relation between the pre-measurement state $\hat{\varrho}$ and the post-measurement state $\tilde{\varrho}$. \square